Measurements from the *RV Ronald H. Brown* and related platforms as part of the Atlantic Tradewind Ocean-Atmosphere Mesoscale Interaction Campaign (ATOMIC)

Patricia K. Quinn[1], Elizabeth J. Thompson[2], Derek J. Coffman[1], Sunil Baidar[3,4], Ludovic Bariteau[2], Timothy S. Bates[1,5], Sebastien Bigorre[6], Alan Brewer[4], Gijs de Boer[2,3], Simon P. de Szoeke[7], Kyla Drushka[8], Gregory R. Foltz[9], Janet Intrieri[2], Suneil Iyer[8], Chris W. Fairall[2], Cassandra J. Gaston[10], Friedhelm Jansen[11], James E. Johnson[1,5], Ovid O. Krüger[12], Richard D. Marchbanks[3,4], Kenneth P. Moran[2,3], David Noone[13], Sergio Pezoa[2], Robert Pincus[2,3], Albert J. Plueddemann[6], Mira L. Pöhlker[12], Ulrich Pöschl[12], Estefania Quinones Melendez[7], Haley M. Royer[10], Malgorzata Szczodrak[10], Jim Thomson[8], Lucia M. Upchurch[1,5], Chidong Zhang[1], Dongxiao Zhang[1,5], and Paquita Zuidema[10]

[1]NOAA Pacific Marine Environmental Laboratory (PMEL), Seattle, WA, USA
[2]NOAA Physical Sciences Laboratory (PSL), Boulder, CO, USA
[3]Cooperative Institute for Research in Environmental Sciences (CIRES), University of Colorado, Boulder, CO
[4]NOAA Chemical Sciences Laboratory (CSL), Boulder, CO, USA
[5]Cooperative Institute for Climate Ocean and Ecosystem Studies (CICOES), University of Washington, Seattle, WA, USA
[6]Woods Hole Oceanographic Institution (WHOI), Woods Hole, MA, USA
[7]Oregon State University, Corvallis, OR, USA
[8]University of Washington, Applied Physics Laboratory (APL), Seattle, WA
[9]NOAA Atlantic Oceanographic and Meteorological Laboratory (AOML), Miami, FL, USA
[10]Rosenstiel School of Marine and Atmospheric Science, University of Miami, Miami, FL, USA
[11]Max Planck Institute for Meteorology, Hamburg, Germany
[12]Max Planck Institute for Chemistry, Mainz, Germany
[13]University of Auckland, Auckland, NZ

Correspondence: Patricia K. Quinn (patricia.k.quinn@noaa.gov)

Abstract. The Atlantic Tradewind Ocean-Atmosphere Mesoscale Interaction Campaign (ATOMIC) took place from January 7 to July 11, 2020 in the tropical North Atlantic between the eastern edge of Barbados and 51°W, the longitude of the Northwest Tropical Atlantic Station (NTAS) mooring. Measurements were made to gather information on shallow atmospheric convection, the effects of aerosols and clouds on the ocean surface energy budget, and mesoscale oceanic processes. Multiple platforms were deployed during ATOMIC including the *NOAA RV Ronald H. Brown* (RHB) (Jan. 7 to Feb. 13) and WP-3D Orion (P-3) aircraft (Jan. 17 to Feb. 10), the University of Colorado's Robust Autonomous Aerial Vehicle – Endurant and Nimble (RAAVEN) Uncrewed Aerial System (UAS) (Jan. 24 to Feb. 15), NOAA- and NASA-sponsored Saildrones (Jan. 12 to Jul. 11), and Surface Velocity Program Salinity (SVPS) surface ocean drifters (Jan. 23 to Apr. 29). The *RV Ronald H. Brown* conducted *in situ* and remote sensing measurements of oceanic and atmospheric properties with an emphasis on mesoscale oceanic-atmospheric coupling and aerosol-cloud interactions. In addition, the ship served as a launching pad for Wave Gliders, Surface Wave Instrument Floats with Tracking (SWIFTs), and radiosondes. Details of measurements made from the *RV Ronald H. Brown*, ship-deployed assets, and other platforms closely coordinated with the ship during ATOMIC are provided here. These platforms include Saildrone 1064 and the RAAVEN UAS as well as the

Barbados Cloud Observatory (BCO) and Barbados Atmospheric Chemistry Observatory (BACO). Inter-platform comparisons are presented to assess consistency in the data sets. Data sets from the *RV Ronald H. Brown* and deployed assets have been quality controlled and are publicly available at the NOAA Physical Sciences Laboratory (PSL) ATOMIC ftp server (ftp://ftp2.psl.noaa.gov/Projects/ATOMIC/data/) and at NOAA's National Centers for Environmental Information (NCEI) data archive (https://www.ncei.noaa.gov/access/metadata/landing-page/bin/iso?id=gov.noaa.nodc:ATOMIC-2020). Point of contact information and links to individual data sets with Digital Object Identifiers (DOIs) are provided herein.

1. Introduction

Shallow, liquid clouds persist at altitudes of hundreds to a few thousand meters above most of the world's oceans. Convection and mixing in the boundary layer can lead to the formation of shallow clouds, which can drive more mixing throughout the cloud layer and result in deeper convection. These clouds reflect incoming solar radiation and lead to a cooling of the surface (Vial et al., 2016). In addition, shallow mixing influences sea surface temperature (SST) and salinity by moderating the air-sea exchanges of energy and moisture (Stevens et al., 2016). Climate models have difficulty accurately representing low clouds in trade-wind regions because many of the processes involved in their formation occur at sub-grid scales (Bony et al., 2015). Improving model performance requires measurements that will result in a better understanding of 1) the boundary layer conditions that lead to cloudiness, 2) the influence of clouds and the atmospheric boundary layer on the upper ocean mixed layer, and in turn, 3) the influence of ocean mixing processes on surface fluxes and the atmospheric boundary layer.

ATOMIC took place in the boreal winter to study shallow convection and low, liquid clouds at a time of year when other cloud types are mostly absent. ATOMIC is the U.S. complement to the Elucidating the Role of Clouds Circulation Coupling in Climate Campaign (EUREC[4]A) (Bony et al., 2017;Stevens et al., 2020). Together, ATOMIC and EUREC[4]A involved 4 research vessels, 4 research aircraft, land-based observations from Barbados, and uncrewed sea-going and aerial vehicles. The ATOMIC - EUREC[4]A study region stretched from the eastern shores of Barbados to the NTAS buoy located ~500 NM to the northeast and south along the coast of South America to ~ 5°N. EUREC[4]A platforms focused on the western portion of the study area while the *RV Ronald H. Brown* and P-3 aircraft worked primarily in the eastern, upwind sector from mid-January to mid-February (Fig. 1). ATOMIC was composed of two legs with Leg 1 conducted between Jan. 7 and 25, 2020 and Leg 2 conducted between Jan. 28 and Feb.13, 2020. NOAA- and NASA-sponsored Saildrones covered the entire study area between January and July 2020. The RAAVEN UAS flew near shore from Morgan Lewis on the eastern side of Barbados between January 24 and February 15. SVPS type surface ocean drifters were deployed from the *RV L'Atalante* and operated along the South American coast (Jan. 23 to Apr. 29).

81 **Figure 1**. Tracks of the *RV Ronald H. Brown,* Wave Gliders, and SWIFTS during ATOMIC (colored by seawater
82 skin T calculated by PSL) for a) Leg 1 and b) Leg 2. Tracks for Wave Gliders, and SWIFTS are magnified in c) Leg
83 1 and d) Leg 2. The portion of the EUREC⁴A study area overlapping with ATOMIC is indicated by the solid green
84 line in b). Locations of *RV Ronald H. Brown* stations, MOVE, and BCO/BACO are also shown in a) and b).
85
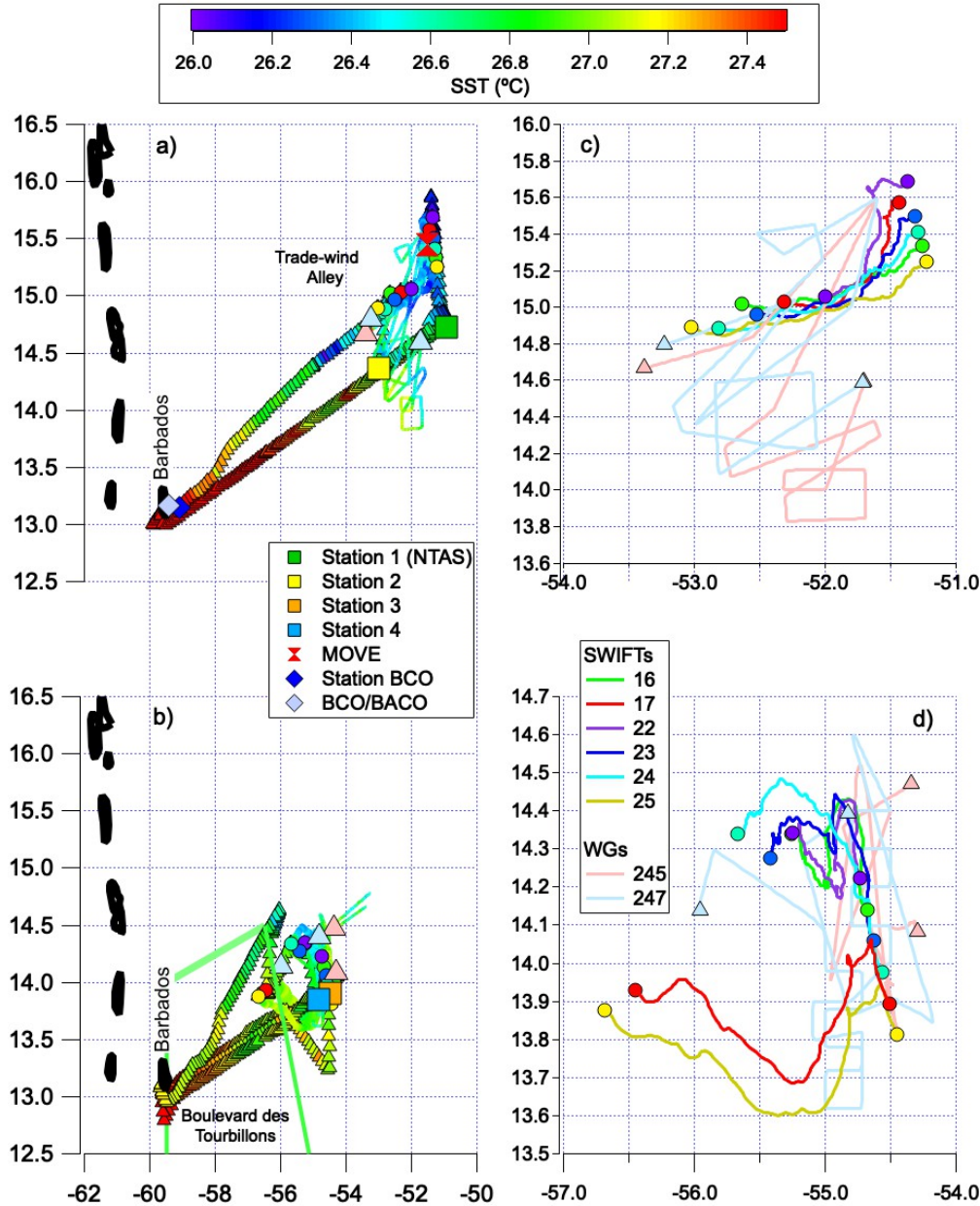
86
87
88 A thorough description of the objectives of ATOMIC and first highlights of the data analyses are presented in
89 Zuidema (2021). A description of data collected from the P-3 is described in Pincus et al. (2021) and data collected
90 by the RAAVEN are documented in de Boer et al. (2021). Here, a detailed overview of the data collected from the
91 *RV Ronald H. Brown* and deployed assets is provided. The goal is to document the sampling strategy,
92 instrumentation used, and data availability to advance the widespread use of the data by the ATOMIC and broader
93 research communities. A description of the sampling strategy, including coordination with other platforms, is

94 described in Sect. 2. Also detailed in Sect. 2 are the measurements made from the *RV Ronald H. Brown,* the NTAS
95 moored buoy, Wave Gliders and SWIFT vessels, Saildrones, RAAVEN UAS, and SVPS drifters. An overview of
96 oceanic and atmospheric conditions sampled is provided in Sect. 3. Results from inter-platform comparisons of
97 atmospheric and oceanic parameters are detailed in Sect. 4. Data availability, format, and quality control are
98 described in Sect. 5 along with links to individual data sets. Available measurement uncertainties are reported in the
99 data set metadata at ftp://ftp2.psl.noaa.gov/Projects/ATOMIC/data/ and
100 https://www.ncei.noaa.gov/access/metadata/landing-page/bin/iso?id=gov.noaa.nodc:ATOMIC-2020.
101

102 **2. Sampling strategy and measurements**
103

104 Sampling onboard the *RV Ronald H. Brown* took place from Jan. 7 to Feb. 13, 2020 and focused on the region

105 between 57°W and 51°W east of Barbados and between 13° and 16°N in the so-called Trade Wind Alley (Fig. 1).

106 The overarching strategy of ATOMIC was to provide a view of the atmospheric and oceanic conditions upwind of

107 the EUREC[4]A study region. Operations of the *RV Ronald H. Brown* were coordinated with the Wave Gliders and

108 SWIFTs deployed from the ship, the P-3 aircraft, Saildrone 1064, and BCO and BACO. An additional logistical

109 objective included recovering the NTAS-17 mooring and replacing it with the NTAS-18 mooring. A third objective

110 was to triangulate and download data from a Meridional Overturning Variability Experiment (MOVE) subsurface

111 mooring and related Pressure Inverted Echo Sounders (PIES). MOVE is designed to monitor the integrated deep

112 meridional flow in the tropical North Atlantic.
113

114 Optimal aerosol and flux measurements were made when the ship was pointed into the wind to avoid contamination

115 by the ship's stack and air flow distortion. Coordinating with the P-3 and Saildrone and deploying the NTAS

116 Mooring, Wave Gliders, and SWIFTs had the advantage of providing redundant and complimentary data streams but

117 the disadvantage of requiring the ship to transit away from the wind for maneuvers. In addition, ship transits to

118 Bridgetown, Barbados for a scheduled in port (Jan. 26 to 28) and a medical emergency (Feb. 3 to 6) were downwind

119 relative to prevailing northeast trade winds. Periods of unfavorable winds for atmospheric sampling were identified

120 by relative winds from behind the ship's beam (~ - 90° through 180° to + 90° relative to the bow at 0°). A time

121 series of relative winds and corresponding high particle number concentrations due to emissions from the ship's

122 stack (~> 1000 cm^{-3}) is shown in Figure 2. These periods have been removed from the aerosol data. Unfavorable

123 sampling conditions were experienced 15% of the time the ship was at sea at the dates and times indicated in Table

124 1. Seawater measurements were less accurate when the ship's speed over water was near zero due to mechanical

125 stirring of the water surface by the ship's propulsion system.
126

127 A general timeline of events for Legs 1 and 2 is provided in Sect. 2.1. and 2.2. Descriptions of the instrumentation

128 onboard the ship and deployed assets are provided in Sect. 2.3 to 2.7 and on the Saildrone, RAAVEN UAS, and

129 SVPS drifters in Sect. 2.8 to 2.10.
130

131

Figure 2. Time series of relative wind direction (apparent wind relative to the bow of the ship, negative values are port and positive values are starboard) and particle number concentration ($D_{gn} > 13$ nm) measured on the *RV Ronald H. Brown* during ATOMIC.
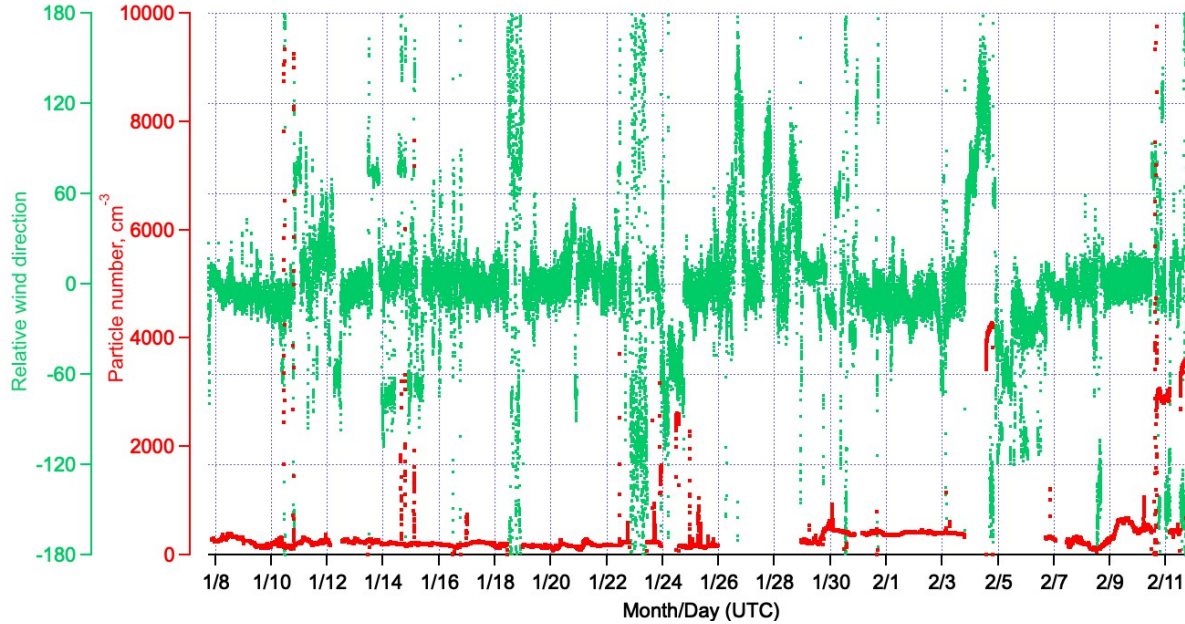
2.1. Sampling events during Leg 1

Timeline of events for Legs 1 and 2 are shown in Table 1. Dates and positions of deployment and recovery of assets are listed in Table 2. Times when platforms were within relatively close proximity providing the potential for inter-platform comparisons are given in Table 3. All times reported throughout the paper are in UTC.

During Leg 1, the NTAS mooring was swapped out, Wave Gliders were deployed for the duration of the experiment, and the SWIFTs were deployed and then recovered at the end of the leg. In addition to these logistical operations, measurements were made throughout the leg to characterize atmospheric and oceanic conditions upwind of the EUREC⁴A study region.

The ship departed Bridgetown, Barbados on Jan. 7, 2020 in transit to the NTAS-18 mooring target location at 14°44'N and 50°56'W. Radiosonde launches every 4 hours and continuous atmosphere and sea surface sampling began early on Jan. 8. The latitude and longitude of the four stations occupied during the cruise are listed in Table 1 and shown in Figure 1. Station 1 (S1) was located in the NTAS region. Two Wave Gliders were deployed on Jan. 9 *en route* to S1. Once at S1, early on Jan. 10 a comparison between shipboard and NTAS-17 atmosphere and ocean measurements was conducted. The NTAS-18 mooring was deployed later on Jan. 10. After deployment, the ship transited 55 NM to the northwest of S1 to the MOVE region near 15°27'N and 51°32'W (Figure 1). Unsuccessful attempts were made over a 24 hr period to triangulate the position of the MOVE1-13 mooring and PIES198 and 238.

157 The ship left the MOVE region on Jan. 12 at 05:30 to transit back to S1. The MOVE work did not compromise

158 continuous atmospheric and surface ocean sampling and is not discussed further.

159

160 **Table 1.** Timeline of sampling events onboard the *RV Ronald H. Brown* (RHB) including coordination with other
161 platforms, NTAS operations, downwind transits, and periods on Station. The different colors shown under RHB
162 correspond to the status of the ship. *NTAS-18 deployed. **NTAS-17 recovered.
163

	Sampling days
	Downwind transit
	In port
	NTAS Operations
	MOVE Operations
C-BCO	Comparison with BCO
C-P3 (Research Flight number)	Coordination with P3
C-SD	Comparison with SailDrone 1064
C-S	Comparison with SWIFTs
C-N17	Comparison with NTAS 17
C-N18	Comparison with NTAS 18
C-RUAS	Comparison with RAAVEN UAS
S1	Station 1 14°44' N, 50°56'W (NTAS area)
S2	Station 2 14º21'44"N, 53ºW
S3	Station 3 13º54'N, 54º30'W
S4	Station 4 13º51'N, 54º51'36"W
Station BCO	Station BCO 13º8'55.7", 59º4'59.2"W

164

	RHB	SWIFTs	WG 245	WG 247	CTD	uCTD	NTAS/MOVE
Jan 7							
8							
9	S1						
10	S1, C-N17						N18*
11							MOVE
12	S1, C-N18						
13	S1, C-N18, C-S						
14	C-S						
15	S1, C-N17						
16	S1, C-N17						N17**
17	S1, C-P3(RF1)						
18	C-P3 (RF2)						
19	S2						
20	S2						
21	S2						
22	C-S						
23	C-P3(RF3)						
24	C-BCO, C-RUAS						
25	C-BCO, C-RUAS						
26							
27							
28							
29							
30	C-S, S3						
31	S3, C-P3(RF5)						
Feb 1	S3						
2	S3						
3	S3, C-P3(RF6)						
4							
5							
6							
7							
8	S4, C-SD, C-P3(RF9)						
9	S4, C-SD						
10	S4, C-SD, C-P3(RF10)						

11	C-S, C-WG, C-P3(RF11)							
12								
13								

165

Table 2. Dates (UTC) and positions of deployment and recovery of NTAS moorings, two Wave Gliders, and six
SWIFTs. Assets are listed in order of start and stop times of the data stream. Distance travelled is given for the
SWIFTs and Wave Gliders.

169

| | Deployment | | Recovery | | |
Asset	Date	Position	Date	Position	Distance (NM)
		LEG 1			
Wave Glider 245	1/9/20 20:55	14° 35' 25" N, 51° 41' 56" W			
Wave Glider 247	1/9/20 20:55	14° 35' 13" N, 51° 42' 21" W			
NTAS-18	1/10/20 17:45	14° 44' N, 50° 56'W			
SWIFT 22	1/14/20 01:13	15° 41' 21" N, 51° 22' 5" W	1/22/20 19:14	15° 3' 29" N, 51° 59' 50" W	52
SWIFT 23	1/14/20 05:11	15° 29' 59" N, 51° 18' 54" W	1/22/20 15:11	14° 57' 47" N, 52° 31' 21" W	62
SWIFT 24	1/14/20 07:11	15° 24' 42" N, 51° 17' 19" W	1/22/20 12:13	14° 53' 12" N, 52° 49' 5" W	94
SWIFT 16	1/14/20 9:11	15° 20' 3" N, 51° 15' 37"	1/22/20 14:13	15° 1' 9", 52° 38' 8"W	82
SWIFT 25	1/14/20 10:12	15° 15' 7" N, 51° 13' 46" W	1/22/20 11:13	14° 53' 26"N, 53° 1' 34" W	60
SWIFT 17	1/14/20 18:11	15° 34' 31" N, 51° 26' 16" W	1/22/20 17:14	15° 1' 55" N, 52° 18' 56" W	60
NTAS-17			1/16/20 10:41	14° 49' 28" N, 51° 00' W	
		LEG 2			
Wave Glider 245			2/7 19:55	14° 4' 55" N, 54° 17' 12" W	153
SWIFT 22	1/30/20 17:12	14° 13' 25" N, 54° 43' 53" W	2/10/20 17:12	14° 20' 35" N, 55° 15' 5" W	31
SWIFT 16	1/30/20 18:13	14° 8' 23" N, 54° 40' 51" W	2/10/20 17:13	14° 20' 28" N, 55° 15' 19" W	36
SWIFT 23	1/30/20 19:12	14° 3' 31" N, 54° 37' 30" W	2/10/20 20:15	14° 16' 30" N, 55° 25' 14" W	48
SWIFT 24	1/30/20 20:13	13° 58' 39" N, 54° 33' 52" W	2/10/20 23:12	14° 20' 19" N, 55° 39' 56" W	68
Wave Glider 247			2/11/20 10:54	14° 8' 11" N, 55° 57' 9" W	248
SWIFT 17	1/30/20 21:10	13° 53' 40" N, 54° 30 '31" W	2/11/20 15:11	13° 55' 47" N, 56° 27' 6" W	127
SWIFT 25	1/30/20 22:13	13° 48' 50" N, 54° 27' 6" W	2/11/20 17:14	13° 52' 37" N, 56° 41' 0.6" W	130

170

Table 3. Times when platforms were within relatively close proximity providing the potential for inter-platform
comparisons. Also given are distances between platforms during the comparisons. Results from inter-platform
comparisons reported here are indicated in bold. Distances between RHB and NTAS refer to distance to the mooring
anchor. Distance to buoys were between 0.25 to 3 NM.

175

Platforms	Start UTC	Stop UTC	Distance (NM)	Comments
RHB, NTAS-17	1/10/20 00:58	1/10/20 08:57	2.5 (mooring anchor)	Station 1
RHB, NTAS-18	**1/12/20 11:30**	**1/13/20 14:00**	**2.9 (mooring anchor)**	**1/12/20 14:06, 19:04; 1/13/20 00:00 CTD casts to 250 m Station 1**
RHB, NTAS-17	**1/15/20 10:00**	**1/16/20 09:05**	**2.9 (mooring anchor)**	**1/15/20 20:16 CTD cast to 5000 m Station 1**
RHB, P-3	1/17/20 14:20		Within dropsonde circle	P-3 RF1, 7.3 – 7.7 km altitude Station 1
RHB, P-3	1/19/20 14:57		Within dropsonde circle	P-3 RF2 7.6 km altitude Station 2
RHB, P-3	1/23/20 14:06, 19:46		Within dropsonde circle	P-3 RF3, 3.2 km altitude 14° 22' 59"N and 55°W Overfly of ship at 150 m at 15:42
RHB, P-3	1/31/20 16:25		Within dropsonde circle	P-3 RF5, 7.4 km altitude Station 3
RHB, P-3	2/3/20 14:13		Within dropsonde circle	P-3 RF6, 7.7 km altitude Station 3
RHB, P-3	2/9/20 05:57		Within dropsonde circle	P-3 RF9, 7.5 km altitude Station 4
RHB, P-3	2/10/20 05:46		Within dropsonde circle	P-3 RF10, 7.5 km altitude Station 4
RHB, P-3	2/11/20			P-3 RF11, 7.5 km altitude

	10:26			Station 4
RHB, SD 1064	**2/8/20 9:30**	**2/10/20 18:50**	**0.7 to 3.6**	**2/8/20 9:30 – 18:10 SD was 2.8 – 3.6 NM upwind, 2/8 19:00 0 2/10 18:50 SD was 0.7 – 0.8 NM from ship Station 4**
RHB, BCO	**1/24/20 18:20**	**1/25/20 23:40**	**20**	**RHB located directly upwind of BCO**

A comparison of atmospheric and oceanic parameters measured onboard the ship and NTAS-18 was conducted Jan. 12 to 13. The comparison included a CTD (conductivity, temperature, and depth) sensor mounted on the ship's rosette and conductivity and temperature sensors attached to the NTAS mooring line. While waiting for the weather to calm down enough to recover NTAS-17, 6 SWIFTs were deployed. The ship transited 55 NM to the northwest and deployed the first SWIFT (22) on Jan. 14 at 01:13 UTC at 15° 41' 21" N, 51° 22' 5" W (Fig. 1, Table 2). Following a southeast track, the remaining 5 SWIFTs were deployed 5 to 12 NM apart across horizontal gradients in ocean surface current and temperature. SWIFT17, the second one deployed, was recovered due to the failure of a 3-D sonic anemometer. The ship returned to SWIFT17 to swap out the anemometer. It was re-deployed near its original position on Jan. 14 at 18:11 UTC. After each SWIFT deployment, underway CTD (uCTD) casts were performed to a depth of 50 m for comparison to SST and salinity measured onboard the SWIFTs and to understand the ocean mixed layer structure at the beginning of each SWIFT Lagrangian drift. In addition, the ship sat near each SWIFT for at least an hour after deployment for a comparison of measured near surface atmospheric and surface sea water parameters.

The ship returned to S1 and conducted a second comparison with NTAS-17 on Jan. 15 to 16, including a CTD cast with the ship's rosette and sensors on the NTAS mooring line. NTAS-17 was recovered on Jan. 16. The ship stayed at S1 and was within the P-3's dropsonde circle during its first flight (Research Flight 1 or RF1) on Jan. 17 from 15:30 to 16:40. A first comparison between the uCTD and the CTD on the ship's rosette for temperature and salinity was conducted on Jan. 17 at 22:36. The ship's CTD cast went to a depth of 500 m.

With the NTAS and MOVE work finished, the ship transited downwind on Jan. 18 for 14.5 hours to Station 2 (S2) located at 14º21'44"N and 53ºW (Fig. 1a). This location was downwind of the projected paths of the SWIFTs but still upwind of the EUREC^{4}A study region. During the transit, aerosol and flux measurements were compromised by relative winds abaft the beam but surface ocean and meteorological measurements as well as radiosonde launches continued. In addition, uCTD casts to 100 m depth were made every hour to investigate a large-scale SST gradient between NTAS and S2. The ship briefly slowed to 2 to 4 kts for each cast.

The ship reached S2 on Jan. 19 at 01:30 UTC and turned into the wind for optimal aerosol and flux measurements. Underway CTDs were conducted to a depth of 100 m every 6 hr. The second overflight of the P-3 (RF2) occurred on Jan. 19 at 14:57 UTC with the *RV Ronald H. Brown* within the aircraft's dropsonde circle. A second comparison between the uCTD and the CTD on the ship's rosette was conducted on Jan. 21 at 16:15 with the ship's CTD reaching a depth of 150 m.

210 On Jan. 22 at 07:30 UTC, the ship left S2 to recover the SWIFTs before the end of Leg 1. The SWIFTs had drifted
211 between 53 and 103 NM to the southwest with those deployed at the more southern locations drifting the furthest
212 (Fig. 1a, Table 2). The ship transited 32 NM to the north to reach the southernmost SWIFT and then followed a
213 course to the northeast recovering the remaining SWIFTs which were 7 to 24 NM apart. Once all SWIFTs were
214 onboard (Jan. 22 19:14), the ship transited 180 NM to the southwest to 14° 22' 59"N and 55°W to be in the center of
215 the P-3's dropsonde circle the next day. Aerosol and flux measurements were compromised during the transit due to
216 the relative wind being abaft the beam.
217
218 The ship reached the designated position on Jan. 23 at 10:30, turned into the wind for optimal aerosol and flux
219 measurements, and was within the P-3's dropsonde circle on Jan. 23 at 14:06 (RF3). Later in the flight (15:42), the
220 P-3 flew over the ship at an altitude of 150 m. This flyby was the closest the P-3 was to the ship during the
221 ATOMIC campaign while all instrumentation was operational. At 22:00 the ship started the 250 NM transit back to
222 Bridgetown with a planned stop upwind of BCO/BACO for a measurement comparison. Initially, relative winds
223 were from the port side of the ship at -100° relative to the bow but 6 hrs into the transit they shifted to a relative
224 direction of -50° due to a change in true wind direction and the ship's course, making for better conditions for
225 aerosol and flux measurements. Radiosonde launches were halted on Jan. 24 at 2:45 near 56°W with the knowledge
226 that sondes launched from the *RV Meteor* and BCO could be used to fill in the gap. The ship arrived at the
227 comparison point 20 NM east of BCO (13° 8' 55.7"N, 59° 4' 59.2"W) at 18:20 on Jan. 24 and stayed until Jan. 25 at
228 23:40 (Fig. 1a). Underway CTDs were conducted approximately every 2 hours until Jan. 25 at 21:58.
229
230 The ship ended Leg 1 with a transit around the southern end of Barbados and into Bridgetown with an arrival on Jan.
231 26 at 12:15 for open house and outreach activities to be conducted on Jan. 27.
232
233 **2.2. Sampling events during Leg 2**
234
235 During Leg 2, the SWIFTs were deployed at the beginning of the leg and then recovered along with the Wave
236 Gliders at the end of the leg. Similar to Leg 1, measurements were made throughout the leg to characterize
237 atmospheric and oceanic conditions upwind of the EUREC[4]A study region.
238
239 The *RV Ronald H. Brown* left Bridgetown at 22:15 on Jan. 28 and headed for Station 3 (S3) located 290 NM to the
240 northeast of BCO/BACO at 13° 54' 0"N and 54° 30' 0"W (Fig. 1b). S3 was roughly halfway between BCO/BACO
241 and NTAS. Radiosonde launches began on Jan. 29 at 6:45 and continued every 4 hrs. The ship veered off its NE
242 track on Jan. 29 at 20:18 and turned to the southeast to map the spatial orientation of SST fronts with gradients
243 around 0.75°C for determining where to deploy SWIFTs. When done with mapping, the ship went north on Jan. 30
244 at 4:15 arriving in the vicinity of S3 and Wave Glider 245 at 08:00. Wave Glider 245 was recovered to replace
245 malfunctioning sensors.
246

247 The ship zigzagged to the northwest and then northeast until reaching 14° 13' 25" N and 54° 43' 53" W on Jan. 30 at

248 17:12 where the first SWIFT deployment of Leg 2 took place (Fig. 1d, Table 2). The remaining SWIFTs were

249 deployed on a southeast track approximately 6 NM apart. After each SWIFT deployment, uCTD casts were

250 performed to a depth of 100 m to provide a subsurface context for SWIFT measurements. During each cast, the ship

251 moved into the wind at 0.5 kts. Wave Glider 245 was re-deployed on Jan. 30 at 18:08 after the last SWIFT was put

252 in the water. The ship then transited back to S3, arriving 5 hrs later at 23:09. During this 6 hr period, as the ship was

253 maneuvering to deploy SWIFTs, relative winds were from the port side between -50 to -100 degrees compromising

254 aerosol and flux measurements.

255

256 The ship remained at S3 until Feb. 3 at 15:00 to characterize diurnal variations in oceanic and atmospheric

257 conditions and to be in position for the P-3's RF5 and RF6. Continuous atmospheric and surface ocean

258 measurements were made, radiosondes were launched every 4 hrs, and uCTD casts were conducted every 2 hrs.

259 Four comparisons between the uCTD and the CTD on the ship's rosette were conducted between Feb. 1 and Feb. 3

260 with the ship's CTD reaching a depth of 400 m. The ship was at the center of the P-3's dropsonde circle on Jan. 31

261 at 16:25 (RF5) and Feb. 3 at 14:13 (RF6).

262

263 On Feb. 3 at 19:30 the ship headed back to Bridgetown for a medical emergency. Aerosol and flux measurements

264 were compromised due to relative winds abaft the beam. Radiosonde launches continued every 4 hours. The last

265 launch before reaching port was on Feb. 4 at 10:45. The ship arrived in Bridgetown on Feb. 4 at 19:00.

266

267 The ship departed Bridgetown on Feb. 6 at 16:00 and headed northeast to Station 4 (S4) located at 13º51'N and

268 54º51'36"W, 21.2 NM southwest of S3. Atmospheric measurements resumed along with radiosonde launches every

269 4 hrs. The ship arrived at S4 on Feb. 8 at 01:00 but left 6 hrs later to recover Wave Glider 245 because it was

270 experiencing navigation problems that could have endangered the vehicle. The Wave Glider was recovered 36 NM

271 to the northeast of S4 (14° 4' 55" N, 54° 17' 12" W) on Feb. 8 at 12:45. Aerosol and flux measurements were

272 compromised during the downwind transit back to S4 between 12:45 and 16:25. Once back on station, optimal

273 aerosol and flux measurements resumed along with uCTD casts every 2 hrs. A CTD cast to a depth of 1000 m with

274 the ship's rosette was conducted on Feb. 8 at 17:00 for comparison to the uCTD.

275

276 Still at S4, the ship was within the P-3's night time dropsonde circle on Feb. 9 (RF9) at 5:57. The NOAA PMEL-

277 operated Saildrone 1064 completed a first leg between BCO and NTAS and then sailed near the ship for a

278 comparison of fluxes and measured meteorological and seawater parameters. The Saildrone was 2.8 to 3.6 NM

279 upwind of the ship between Feb. 8 from 9:30 to 18:10 and within 0.7 to 0.8 NM of the ship between Feb. 8 19:00

280 and Feb. 10 18:50. Two final comparisons between the uCTD and the CTD on the ship's rosette were conducted on

281 Feb. 8 and Feb. 9 with the ship's CTD going to depths of 1000 and 400 m, respectively. The ship remained at S4 for

282 the P-3's second night flight (RF10) and was within the dropsonde circle on Feb. 10 from 05:46 to 06:42. The ship's

283 final coordination with the P-3 occurred during a combination research and sightseeing flight with press (RF11) on

284 Feb. 11. The ship was not within the dropsonde circle but was flown over at sunrise at 10:26.

285

286 The ship remained at S4 until Feb. 10 at 12:00 at which point aerosol measurements were ended and the ship began

287 the transit to recover SWIFTs and Wave Glider 247. Recovery operations were conducted between Feb. 10 15:00

288 and Feb. 11 18:15. The four SWIFTs (16, 22, 23, and 24) that were initially deployed to the north between 14° 13'

289 25" and 13° 58' 39" N drifted to the northwest travelling a total distance ranging from 31 to 68 NM (Table 2, Fig.

290 1b). The two SWIFTs (17 and 25) deployed to the south between 13° 53' 40" N and 13° 48' 50" N initially drifted to

291 the southwest, each traveling 130 NM. The ship transited to the northeast to pick up the northern cluster of SWIFTs

292 first, staying near each asset for up to 1.5 hrs for a comparison of measured atmospheric and oceanic parameters.

293 The ship then did several back-and-forth tracks between the position of Wave Glider 247 and SWIFT 17 mapping a

294 SST front before recovering the Wave Glider and the last two SWIFTs.

295

296 After the SWIFTs and Wave Glider were recovered, the ship started a northeast transit on Feb. 11 around 19:30

297 across a SST front in the upwind direction to study air-sea interaction and atmospheric and oceanic mixed layer

298 variability. Underway CTDs were made continuously. On Feb. 12 at 06:00, the ship began the southwest transit back

299 to Bridgetown for the final time. Atmospheric sampling was compromised during the downwind transit. The last

300 radiosonde launch occurred on Feb. 12 at 10:45. The ship arrived in port on Feb. 13 at 10:00.

301

302 **2.3. NTAS operations and measurements**

303

304 NTAS was established to provide accurate air-sea flux estimates and upper ocean measurements in a region with

305 strong SST anomalies and the likelihood of significant local air-sea interaction on interannual to decadal timescales

306 (Weller, 2018;Bigorre and Galbraith, 2018). The station is maintained at a site near 15°N and 51°W through

307 successive mooring turnarounds. During Leg 1, the Upper Ocean Processes Group of the Woods Hole

308 Oceanographic Institution (WHOI) and crew of the *RV Ronald H. Brown* deployed the NTAS-18 mooring and

309 recovered the NTAS-17 mooring at nearby sites. Both moorings used Surlyn foam buoys as the surface element.

310 These buoys are outfitted with two Air–Sea Interaction Meteorology (ASIMET) systems (Colbo and Weller, 2009).

311 The ASIMET system measures, records, and transmits via Iridium satellites the surface meteorological variables

312 necessary to compute air–sea fluxes of heat, moisture and momentum. The upper 160 m of the mooring line are

313 outfitted with oceanographic sensors for the measurement of temperature, salinity and velocity. Information on the

314 instruments providing real-time data, measured atmospheric and oceanic parameters, and height/depth of the

315 measurements on the NTAS mooring are provided in Table 4.

316

317

318   **Table 4.** Instrumentation providing real-time data onboard the NTAS mooring.

Instrument	Measured/derived quantities, raw sampling interval	
	Atmospheric parameters	**Height (m)**
ASIMET system	Bulk air-sea fluxes, relative humidity, temperature, pressure, wind speed and direction, precipitation rate, longwave radiation, shortwave radiation, 1 min	3
	Oceanic parameters	**Depth (m)**
ASIMET system	Sea surface temperature and salinity, 1 min	0.8
Seabird (SBE-37 IM)	Temperature and salinity, 5min	10
NORTEK Aquadopp	Currents, 20 min	13
Seabird (SBE-37 IM)	Temperature and salinity, 5min	25
Seabird (SBE-37 IM)	Temperature and salinity, 5min	40
Seabird (SBE-37 IM)	Temperature and salinity, 5min	55
Seabird (SBE-37 IM)	Temperature and salinity, 5min	70

319

320

321   ASIMET data are sampled and recorded internally every minute. The oceanographic measurements are recorded

322   either every 5 min or 10 min for temperature and salinity (depending on the instrument type) and 20 min or 1 hr for

323   currents. The NTAS-18 mooring was deployed on Jan. 10 at 14° 44' N, 50° 56' W with anchor drop at 17:45 in

324   5055 m of water. The NTAS-17 mooring was recovered on Jan. 16 with anchor release at 10:41. Both buoys have a

325   watch circle of about 2 NM from their respective anchors and were separated by about 6 NM during the January 10

326   to 16 period allowing for comparisons of measured ocean and atmosphere parameters. Atmospheric data from

327   NTAS-17 and NTAS-18 were combined for comparison to measurements onboard the *RV Ronald H. Brown* (Sect.

328   4.2.1).Wind speed, air temperature, and specific humidity were adjusted to a height of 10 m and neutral atmospheric

329   stability using the COARE 3.6 bulk model for the comparison (Fairall et al., 2003;Edson et al., 2013). NTAS data in

330   the ATOMIC archive only include data collected during the ATOMIC campaign.

331

332   On Apr. 8, 2020 at 08:00 UTC, the NTAS-18 buoy went adrift. It meandered slowly toward the Caribbean for 7

333   months until being recovered on Oct. 20, 2020. NTAS-19 was deployed on Oct. 22, 2020.

334

335   **2.4. Shipboard atmospheric measurements**

336

337   Instrumentation onboard the *RV Ronald H. Brown* for the measurement of atmospheric and aerosol parameters is

338   listed in Table 5. Locations of instruments on deck are shown in Figure 3. NOAA's Physical Science Laboratory

339   (PSL) collected data to enable a deeper understanding and quantification of cloud processes, the environments in

340   which they either grow or dissipate, how the ocean and atmosphere interact, and the spatial variability of these

341   processes. Instrumentation mounted on the bow mast and forward O2 deck (two levels above the main deck)

342   measured sea-surface meteorological properties, rain rate, radiative fluxes, and air-sea turbulent fluxes using bulk,

343   eddy covariance, and inertial dissipation methods (Fairall et al., 1997;Fairall et al., 1996;Fairall et al., 2003;Edson et

344   al., 2013). Vertical profiles of backscatter from a ceilometer mounted on the forward O3 deck (three levels above the

345   main deck) provided cloud base height and temporal cloud fraction. For comparison with other platforms (NTAS

346   and Saildrone 1064), wind speed, air temperature, air pressure, and specific humidity were adjusted to a height of 10

347 m using the COARE 3.6 bulk algorithm. Final data products of meteorological and navigation data are 1-min and

348 10-min averages of high-resolution raw data (see Table 5 for raw sampling intervals). The data are time-stamped at

349 the beginning of the 1- and 10-min period. Fluxes were calculated at 10-min resolution, then interpolated to 1-min.

350

351 University of Miami (UM) provided high resolution measurements of cloud and rain to better understand the

352 relationship between cloud properties and cloud spatial organization as a function of cloud mesoscale organization,

353 in particular rain and the associated atmospheric cold pools (Stevens et al., 2020;Löffler-Mang and Joss, 2000). Two

354 collocated Parsivel disdrometers mounted on the forward O3 deck provided precipitation intensity, drop number,

355 and equivalent radar reflectivity. A sky camera provided a 50° field of view oriented horizontally off the starboard

356 side of the ship every 4 sec. A microwave radiometer was deployed to provide cloud liquid water path estimates but

357 its data acquisition was unsuccessful and no data are available. A Marine Atmospheric Emitted Radiance

358 Interferometer (M-AERI) was mounted on the port side O2 deck rail (2 levels above the main deck) (Minnett et al.,

359 2001). It measured the spectra of infrared emission from the sea surface and atmosphere for the derivation of skin

360
361 **Table 5**. Instrumentation onboard the *RV Ronald H. Brown* for the measurement of atmospheric and aerosol
362 parameters. The O2 and O3 decks were two and three levels above the main deck, respectively. [a]Aerosol inlet was
363 located on the O2 deck, 18 m.a.s.l. Final data products of meteorological and navigation data are 1-min and 10-min
364 averages of high-resolution raw data and time-stamped at the beginning of the 1- and 10-min period. Fluxes were
365 calculated at 10-min resolution, then interpolated to 1-min for those files.
366

Instrument	Measured/derived quantities, raw sampling interval	Location
Atmospheric parameters		
Gill WindMaster Pro 3-axis ultrasonic anemometer	Wind vector, stress, and sensible heat flux, 0.1 sec	Bow mast
Optical precipitation sensor, OSI Inc., ORG-815 DA	Rain rate, 5 sec sampling, collected/recorded every 1 min	Bow mast
Li-COR 7500 Gas Analyzer	Water vapor density, turbulent latent heat flux, 0.1 sec	Bow mast
Vaisala HMT335	Air temperature, humidity, 1 min	Bow mast
Vaisala PTB220	Atmospheric pressure, 1 min	O2 deck
2 Eppley PSPs (Pyranometer)	Shortwave radiation, 1 min	O2 deck
2 Eppley PIRs (Pyrgeometer)	Longwave radiation, 1 min	O2 deck
Systron and Donner MP-1 6-axis motion detector system	3-D ship acceleration, 0.1 sec	Bow mast
Vaisala CL31 Ceilometer	Vertical profiles of backscatter from refractive index gradients, cloud base height, cloud fraction, 15 sec sampling from 0-7.7 km with 10 m vertical spacing	O3 deck
2 Parsivel optical rain gauges, 650 and 780 nm	Rain rate, equivalent radar reflectivity, particle number	O3 deck
StarDot Camera, NetCam XL	Pointed to starboard, field of view of 50°, image captured every 4 sec	O3 deck
Doppler lidar λ=1.5 μm	Atmospheric vertical velocity and backscatter intensity, horizontal wind profiles, estimates of cloud base and mixed layer heights; 0.5 sec	O2 deck
W-band (95.56 GHz) Doppler vertically pointing cloud radar	Vertical profiles of non-precipitating and lightly-precipitating clouds from 100 m to 4.2 km with 30 m vertical resolution every 0.5 sec	O2 deck
Dual-flow, two filtered radon detector	^{222}Rn, 30 min	O3 deck
Vaisala WXT536	T, RH, rain rate; 1 sec	O2 deck
Picarro water vapor isotope analyzer (L2130-fi)	Water vapor concentration and isotopic composition, 0.2 sec	Aerosol inlet[a]
Vaisala RS-41 radiosondes	Profiles of T, RH, P, and winds every 4 hrs	Main deck
Thermo Environmental Model 49C	Ozone, 1 sec	Inlet at 18 m.a.s.l.
Aerosol Properties		
Collection with multi-jet cascade impactors and analysis by ion chromatography, thermal-optical, gravimetric, and XRF analysis	Size segregated concentrations of Cl⁻, NO$_3$⁻, SO$_4$⁼, methanesulfonate (MSA⁻), Na⁺, NH$_4$⁺, K⁺, Mg^{+2}, Ca^{+2}, organic carbon, elemental carbon, trace elements; hours	Aerosol inlet[a]

DMPS and TSI 3321APS	Number size distribution 0.02 to 10 μm, 5 min	Aerosol inlet[a]
TSI 3025A, 3760A, 3010	Number concentration > 3, 13, 13 nm; 1 sec	Aerosol inlet[a]
TSI 3563 Nephelometer	Sub-1.1 and sub-10 μm light scattering and backscattering; 450, 550, 700 nm; 60% RH; 1 sec	Aerosol inlet[a]
TSI 3563 Nephelometers	Sub-1.1 μm scattering f(RH); 450, 550, 700 nm; dry and 80%RH; 1 sec	Aerosol inlet[a]
Radiance Research PSAP	Sub-1.1 and sub-10 μm light absorption; 467, 530, 660 nm; dry	Aerosol inlet[a]
DMT CCNC	Sub-1.1 μm cloud condensation nuclei concentration, 0.1 to 0.6% S, 1 sec	Aerosol inlet[a]
Solar Light Microtops Sunphotometer	Aerosol Optical Depth; 380, 440, 500, 675, 870 nm	O3 deck

367
368
369
370
371
372
373
374

375 **Figure 3.** Instrumentation onboard the *RV Ronald. H. Brown* for the measurement of atmospheric and oceanic
376 parameters located on a) the bow mast and forward O2 deck and b) port side O3 deck. Asset deployments are shown
377 for c) NTAS mooring, d) ship's rosette with CTD and Niskin bottles, e) uCTD, f) SWIFT, g) Wave Glider, and h)
378 radiosonde. Also shown are i) P-3 fly over of the ship on Jan. 23 and j) Saildrone upon its return to the U.S.
379 (Newport, RI) from Barbados. Not shown are disdrometers on the port O3 deck and camera on the starboard O3
380 deck.

381
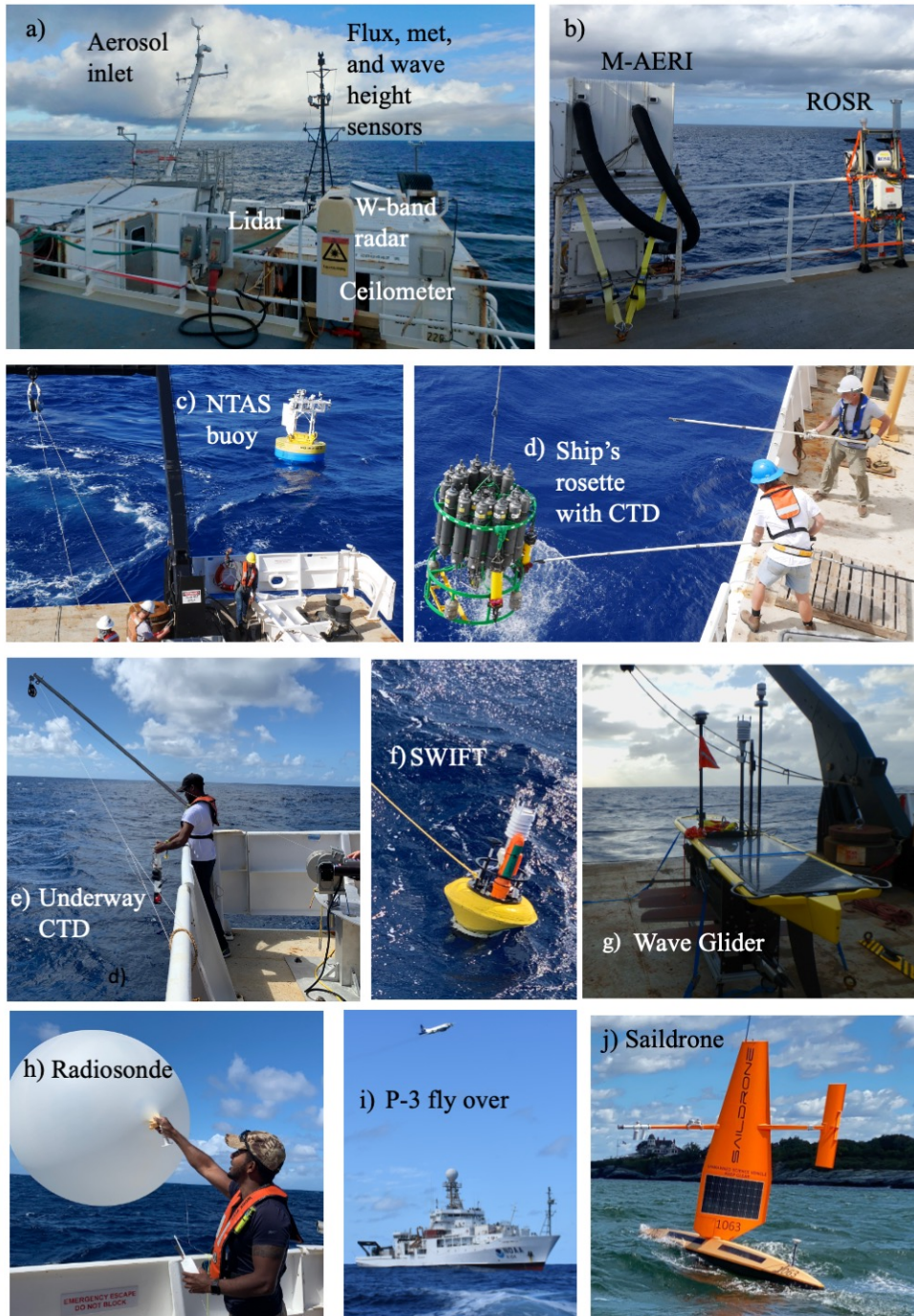
382   sea surface temperature and lower troposphere profiles of temperature and humidity (Szczodrak et al., 2007). A W-

383   band Doppler vertically pointing cloud radar was housed in a container on the O2 deck for the measurement of

384   vertical profiles of non-precipitating and lightly-precipitating clouds (Moran et al., 2012). The radar was not

385   functional during Leg 1 and operated with a 10 dB attenuator on Leg 2 that prevented detection of non-precipitating

386   clouds. Although the loss of this information limited the ship-based based observations of non-precipitating cloud,

387   data from the shipboard ceilometer and Doppler radar and the cloud radar on the P-3 will be used to fill in gaps.

388

389   NOAA's Chemical Sciences Laboratory (CSL) operated a microjoule class, pulsed Doppler lidar (microDop)

390   operating at a wavelength of 1.5 μm to assess atmospheric turbulence, aerosol backscatter intensity, and horizontal

391   winds (Schroeder et al., 2020). The lidar was mounted on the forward O2 deck. The system was motion stabilized

392   while staring vertically to within 0.25 degrees of zenith. Ship motion projected onto the line-of-site velocity

393   measurement was estimated and removed using a 6-axis inertial navigation unit (INU). The INU allowed the lidar to

394   measure the mean and turbulent motions of aerosol in clear air and cloud scatterers with a spatial and temporal

395   resolution of 33.6m and 2Hz respectively. The first valid gate was 75m above the ocean surface. The maximum

396   height of valid data depends on the availability of aerosol scattering targets. Typically, the instrument provided data

397   through the top of the marine atmospheric boundary layer, in the presence of elevated dust layers to 3 km, and

398   clouds to a height of 7 km. The lidar pointed vertically 95% of the time to sample updrafts and downdrafts in the

399   subcloud mixed layer and in the interstitial trade cumulus boundary layer and spent 2 minutes of every hour

400   performing a 65° elevation, full azimuthal scan to measure horizontal wind profiles. Real-time quicklooks of

401   backscatter intensity profiles showing strongly scattering cloud base and updraft structures were available for

402   awareness of the clouds and turbulent mixed layer throughout the cruise. Cloud base height (CBH) was retrieved by

403   applying Haar wavelet covariance transforms to the backscatter intensity profiles.

404

405   Oregon State University and the National Center for Atmospheric Research (NCAR) operated a Picarro water vapor

406   isotope analyzer on Leg 2 of the cruise to investigate processes that shape the atmosphere's humidity structure and

407   its variations. The spectroscopic analyzer measured water vapor concentration and its isotopic composition, the

408   isotope ratios of oxygen ($^{18}O/^{16}O$) and hydrogen (D/H). All three quantities were measured continuously at 5 Hz

409   frequency via the aerosol inlet on the O2 deck at 18 m above sea level (m.a.s.l.). Complementary gas-phase water

410   isotopic measurements were made from the P-3, at BCO, from the French ATR aircraft, and aboard German and

411   French research vessels. Rainwater and seawater were also collected from the ship platforms for future offline

412   analysis. Surface sea water and water column samples from CTD casts were also collected to investigate the upper

413   ocean mixing and the freshwater balance to be evaluated in the context of air-sea gas exchange and upper ocean

414   circulation.

415

416   The goals of NOAA's Pacific Marine Environmental Laboratory (PMEL) were to assess the impacts of aerosols on

417   clouds and direct aerosol light scattering and absorption on the temporal variability of net radiation reaching the

418   ocean surface and SST for the conditions of a well-mixed boundary layer. Measurements included aerosol chemical

composition, total number concentration, number size distribution, light scattering and its dependence on relative humidity, light absorption, and cloud nucleating ability. Aerosol instrumentation was housed in two containers on the O2 deck. All instruments drew sample air from an inlet 18 m.a.s.l. mounted on top of one of the O2 deck vans (Bates et al., 2002) (Fig. 3). Aerosol optical depth (AOD) was measured using Microtops hand held sunphotometers. The raw Microtops data were processed by the NASA Maritime Aerosol Network in conjunction with the Aerosol Robotic Network (Smirnov et al., 2009). In addition, ^{222}Rn was measured for its use as a tracer of continentally-influenced air masses (Whittlestone and Zahorowski, 1998) and O_3 was measured for its use as an indicator of entrainment from the upper troposphere.

Radiosondes were launched throughout the ATOMIC campaign to provide information about the temporal evolution and vertical structure of the boundary layer, upper atmosphere, and clouds. A total of 97 radiosondes (Vaisala RS41-SGP) were launched from the fantail during Leg 1 and 66 were launched during Leg 2. There were 6 launches per day at 02:45, 06:45, 10:45, 14:45, 18:45, and 22:45 UTC. Vertical profiles of pressure, temperature, relative humidity, and winds were measured from the surface to approximately 25 km. Measurements were also made during the radiosondes' descent. Data were communicated to the Global Telecommunications System (GTS) following each sounding via email to the U.S. National Weather Service and via FTP to MeteoFrance. The data were put into 10 m altitude bins and merged with the EUREC^{4}A sounding network. Raw (Level-0), quality-controlled 1-second (Level-1), and vertically gridded (Level-2) data in NetCDF format are available to the public at AERIS (https://doi.org/10.25326/62). The methods of data collection and post-processing can be found in (Stephan et al., 2020).

Radiosonde operations were suspended on the ship west of ~56°W when the ship transited to Bridgetown for the planned in port (Jan. 24 at 2:45) and an emergency medical evacuation (Feb. 4 at 10:45). Soundings from BCO were stitched together with those from the ship to allow for an uninterrupted data record over the entire cruise.

The Lifted Condensation Level (LCL) was calculated from the BCO-RHB radiosonde data record and assumed to represent Cloud Base Height (CBH). The LCL (in m) was calculated as

$$LCL = (T_{50} - T_{d,50}) \times 125 + 50 \qquad (1)$$

where T_{50} is temperature and $T_{d,50}$ is dew point, both at 50 m height (Espy, 1836; Bolton, 1980). The lowest altitude considered was 50 m to avoid contamination by the temperature and relative humidity near the ship's deck and to minimize the effect of vertical gradients in the surface layer. Since the calculation started at 50m, 50 was added to the LCL.

2.5. Shipboard oceanic measurements

456   Instrumentation onboard the *RV Ronald H. Brown* for the measurement of oceanic parameters is listed in Table 6.

457   Locations of instruments mounted on the deck are shown in Figure 3. As stated above, UM's M-AERI, located on

458   the port side forward O2 deck, measured sea surface skin temperature (Minnett et al., 2001).

459

460   **Table 6**. Instrumentation onboard the *RV Ronald H. Brown* for the measurement of seawater parameters. O2 deck is
461   two levels above the main deck.
462

Instrument	Measured /derived quantities, raw sampling interval	Location
Marine Atmospheric Emitted Radiance Interferometer (M-AERI)	Sea surface skin temperature, 5 – 7 min averages	O2 deck
Remote Ocean Surface Radiometer (ROSR)	Sea surface skin temperature, 5 min averages	O2 deck
Floating YSI 46040 Thermistor (Sea snake)	Sub-skin sea surface temperature, ~ 0.05 m depth, 1 sec	Deployed off port side with outrigger
Riegl 1-D laser altimeter	Wave height and period, 10 min averages	Bow mast
Seabird 9+ CTD	At station conductivity (salinity), temperature, depth (pressure), PAR, fluorescence, and oxygen	Deployed off starboard side, main deck
Seabird SBE45 thermosalinigraph Seabird SBE38 thermistor	Seawater temperature, conductivity (salinity), 1 sec	5.3 m below the surface
Acoustic Doppler Current Profiler 75 kHz (ADCP)	Current velocity across 2 depth ranges depending on mode. Narrowband: 29-892 m. Broadband: 17-333 m. 5 min sampling.	Ship's hull
RBR Concerto underway CTD + Tuna Brute winch (uCTD)	Conductivity (salinity), temperature, and depth (pressure) from the surface to 60 or 130 m depending on cast	Deployed off starboard aft quarter

463

464   During Leg 1, the Applied Physics Laboratory at the University of Washington (APL-UW) also measured sea

465   surface skin temperature with a Remote Ocean Surface Radiometer (ROSR) located near the M-AERI. PSL

466   measured sub-skin temperature at approximately 0.05 m depth with a floating thermistor (a.k.a sea snake) deployed

467   off the port side. A skin temperature value was estimated by the COARE algorithm using the sea snake data as input

468   (Fairall et al., 1996;Fairall et al., 1997). This algorithm accounts for the cool skin present in the upper ~0.2-1 mm

469   and any potential diurnal warm layers in the upper ~10 m. This COARE-calculated skin T and the current-relative

470   wind were used to compute bulk, eddy covariance, and inertial dissipation air-sea fluxes (Fairall et al., 1997;Fairall

471   et al., 2003). The COARE 3.6 algorithm estimated wave parameters using wind as input. The parameterization is

472   based on fits to the Banner and Morison (2010) wave model and the flux database collected by NOAA PSL,

473   University of Connecticut, and Woods Hole Oceanographic Institution (Fairall et al., 2003;Edson et al., 2013). PSL

474   also measured significant wave height and period with a 1-dimensional downward looking RIEGL laser altimeter

475   mounted on the bow mast.

476

477   The ship's rosette-mounted CTD was intermittently deployed off the starboard main deck for comparison to the

478   uCTD, Wave Gliders, SWIFTs, and NTAS moorings. Water was collected from the Niskin bottles for analysis of the

479   isotopic composition of oxygen and hydrogen. In addition, the ship had an underway seawater sampling system

480   consisting of a thermistor SBE38 located at the intake valve on the hull and a thermosalinograph SBE45 located

481   inside the ship. These sensors produced underway measurements of temperature and conductivity (salinity) from

482   water sampled at ~5.3 m below the surface. The values recorded may be representative of seawater properties

483   shallower in depth due to an unknown amount of mixing along the hull of the ship that is dependent on currents,

484 ship speed, and waves. The ship also had a 75 kHz acoustic Doppler current profiler (ADCP) for the measurement of
485 currents at depths greater than ~ 17 m.
486
487 UW deployed an underway CTD (uCTD) for the measurement of conductivity (salinity), temperature, and pressure
488 (depth) to assess variability in the upper 60 to 130 m of the water column (Mojica and Gaube, 2020). The uCTD was
489 deployed off the starboard aft quarter. Initially, the probe was lowered by hand with line pre-measured to 50 m.
490 Casts were completed more frequently and with an electric winch after the NTAS mooring work was done which
491 freed up deck space. During Leg 2, a cast with the ship's CTD was conducted every day at 13:00 (Jan. 31, Feb. 1
492 and 2) or 17:00 (Feb. 3, 8, and 9) shortly after a uCTD cast. These casts were used to correct the uCTD conductivity
493 data which had a small offset due to interference from the sensor guard. A transect of intensive uCTD data was
494 collected when the ship transited from NTAS (S1) to S2 on Jan. 18. While at S2, uCTD casts were conducted every
495 1 to 4 hrs. In addition, uCTD casts were conducted every 2 hrs during the majority of Leg 2 when the ship was
496 stationary. The frequency of uCTD sampling increased to every 10 min between 13:00 and 15:15 on Feb. 9 to study
497 heaving of periodic internal waves located at the base of the mixed layer (60-80 m depth) and for 7 hrs at the end of
498 Leg 2 on Feb. 11 and 12 as the ship transited across a strong SST front in the upwind direction. uCTD casts were
499 also performed when deploying or recovering the SWIFTs and Wave Gliders for comparison purposes.
500
501 **2.6. Wave Glider measurements**
502
503 Two Wave Gliders (serial numbers 245 and 247) operated by APL-UW were deployed within 15 minutes of each
504 other on Jan. 9 (Fig. 1a and Table 2). The Wave Gliders greatly increased the sampling of spatial inhomogeneities in
505 atmospheric and oceanic properties as well as bulk air-sea fluxes in the study area (Thomson and Girton,
506 2017;Thomson et al., 2018). The deployment occurred on the transit to NTAS approximately 45 NM to the
507 southwest of the buoy with the intent of leaving the Wave Gliders in the water throughout the length of the cruise.
508 They were remotely piloted from shore via an online portal to cross gradients in SST and ocean currents. Data were
509 available in near real time which helped guide their course. The Wave Gliders were equipped with surface
510 meteorological sensors (bulk winds, air temperature, relative humidity, pressure, and longwave and shortwave
511 radiation), sky cameras, wave motion sensors, downward looking ADCPs for currents, and CTDs at 1 and 8 m depth
512 for conductivity (salinity) and temperature measurements at 1 and 8 m depth. Measurements were collected during
513 20-min bursts every 30 min. Final data products are 60-min averages of high-resolution raw data within each hour,
514 time-stamped at the beginning of the hour. Instrumentation onboard the Wave Gliders is listed in Table 7.
515
516 Wave Glider 245 was recovered, repaired, and redeployed on Jan 30. Telemetered data suggested that the humidity
517 sensor had malfunctioned. When recovered, it was found that the radiometers and their entire mounting pole were
518 gone, water was inside the data logger housing, the Airmar meteorological sensor and light were broken, and the
519 Vaisala meteorological sensor was destroyed. The radiation measurements lasted approximately one week into the
520 deployment. The Wave Glider was redeployed with spare Vaisala and Airmar meteorological sensors but no

521   radiometer. Wave Glider 245 was recovered for the final time on Feb. 7 because it was experiencing navigation

522   problems that could have endangered the vehicle. Wave Glider 247 sampled from Jan. 9 to Feb. 11. On Jan. 31,

523   Wave Glider 247 was inspected with the ship at close range after finding Wave Glider 245 damaged the day before.

524   The meteorological sensors were found to be in good condition but the radiometers had detached and were being

525   dragged by wires on the port side of vehicle. A small boat was deployed to clip the radiometer wires and take the

526   instruments back to the ship.

527

528 **Table 7**. Instrumentation onboard the Wave Gliders for the measurement of atmospheric and seawater parameters.
529 Data were collected during bursts lasting 20 min at the top of each hour. Measurements were collected during 20-
530 min bursts every 30 min. Final data products are 60-min averages of high-resolution raw data within each hour and
531 time-stamped at the beginning of the hour.

Instrument	Measured quantity	Height (+) Depth (-) (m)	Raw sampling interval
Airmar 200WX	Wind velocity (true and relative), GPS position, COG, SOG, magnetic heading, temp, pressure, pitch and roll	+1.3	1 sec
Vaisala WXT530	Wind velocity, air temperature, pressure, relative humidity, rain rate	+1	1 sec
Kipp Zonen CMP3 pyranometer	Short wave radiation (300-2800 nm)	+1	5 sec
Kipp Zonen CGR3 pyrgeometer	Long wave radiation (4200-4500 nm), temperature of sensor	+1	5 sec
GPSWaves/Microstrain 3DM-GX3-35 GPS/AHRS	Directional (2D) wave spectra, and standard bulk wave parameters of height, period, direction	0	0.25 sec
Aanderaa 4319	Conductivity, temperature	-0.24	2 sec
RDI Workhorse Monitor 300kHz ADCP	Ocean current profiles with 4 m vertical resolution	data between -6 to -100 m	1 second pings, ensemble averages recorded every 2 min
Seabird GPCTD+DO	Conductivity, temperature, depth, dissolved O2	-8 m	10 sec

532

533

2.7. SWIFT measurements

535

536   Drifting with ocean currents and winds, the SWIFTs (Surface Wave Instrument Floats with Tracking) offered a

537   Lagrangian view of the near-surface ocean and atmospheric properties, ocean waves and currents, bulk air-sea

538   fluxes, and cloud features (Thomson, 2012;Thomson et al., 2019). Instrumentation onboard SWIFTs v4 and v3 is

539   listed in Tables 8 and 9, respectively. Six SWIFT drifters were deployed in two SE-NW lines across gradients in

540   SST and ocean surface currents – once during Leg 1 and once during Leg 2. These gradients were identified with

541   satellite MUR v4 SST daily plots and the ship's underway thermistor, thermosalinograph, and ADCP. Two version 3

542   (serial number 16 and 17) and four version 4 (serial number 22, 23, 24, and 25) SWIFTs were deployed. All had

543   bulk meteorological sensors (winds, air temperature and pressure on all models, plus relative humidity on the v4

544   models), sky cameras, and CTD sensors at 0.3 m depth for measuring temperature and conductivity (salinity). The

545   v3 models also had conductivity and temperature sensors at 1.1 m depth. The v3 SWIFTs measured ocean

546 turbulence in the upper 0.62 m. The v4 SWIFTs measured ocean turbulence in the upper 2.64 m. Both versions had

547 ADCPs that measured vertical profiles of currents down to 20 m. The SWIFTs sampled high resolution bursts of

548 data for 8 min at the top of each hour. These data were archived on board the vehicle for final processing once

549 recovered. The 8-min data segments and platform location were also averaged and reported via Iridium satellite

550 telemetry each hour for monitoring purposes. SWIFT locations were also tracked in real time using the AIS ship

551 traffic system (local VHF radio signals). The SWIFTs were deployed for 8 days during Leg 1 (Jan. 14 to 22) and 13

552 days during Leg 2 (Jan. 30 to Feb. 11).

553

554 **Table 8**. Instrumentation onboard the version 4 SWIFTs (serial numbers 22, 23, 24, 25) for the measurement of
555 atmospheric and seawater parameters. Measurements were collected during 8-min bursts at the beginning of each
556 hour. Final data products are 8-min averages of high-resolution raw data, time-stamped at the beginning of each
557 hour.

Instrument	Measured quantity	Height (+) Depth (-) (m)	Raw sampling interval
Vaisala WXT530	Wind velocity, air T, barometric pressure, relative humidity, rain rate	0.5	1 sec
Camera	320 x 240 JPEG cloud images	0.2	4 sec
SBG Ellipse GPS/AHRS	Directional (2D) wave spectra, and standard bulk wave parameters of height, period, direction	0	0.2 sec
Nortek Signature 1000 ADCP with AHRS	Turbulent kinetic energy dissipation rate profiles with 0.04 m vertical resolution	-0.3 to -2.64	0.25 sec
	Ocean current profiles with 0.5 m vertical resolution	-0.35 to -20	0.25 sec
	3-D motion and heading data	0	0.25 sec
Aanderaa 4319	Conductivity (salinity), temperature	-0.3	2 sec

558
559

560 **Table 9**. Instrumentation onboard the version 3 SWIFTs (serial numbers16 and 17) for the measurement of
561 atmospheric and seawater parameters. Measurements were collected during 8-min bursts at the beginning of each
562 hour. Final data products are 8-min averages of high-resolution raw data and time-stamped at the beginning of the
563 hour.

Instrument	Measured quantity	Height (+) Depth (-) (m)	Raw sampling interval
Airmar 200WX	Wind velocity, GPS position, COG, SOG, magnetic heading, air temperature and pressure, pitch and roll	0.8	1 sec
Camera	320 x 240 JPEG cloud images	0.2	4 sec
GPSWaves/Microstrain 3DM-GX3-35 GPS/AHRS	Directional (2D) wave spectra, standard bulk wave parameters of height, period, direction	0	0.25 sec
Nortek Aquadopp ADCP	Turbulent kinetic energy dissipation rate profiles with 0.04 m vertical resolution	-0.02 to -0.62	0.25 sec
	Ocean current profiles with 0.5 m vertical resolution	-0.65 to -20	0.25 sec
Aanderaa 4319	Conductivity (salinity), temperature	-0.50	2 sec
Aanderaa 4319	Conductivity (salinity), temperature	-1	2 sec

2.8. Saildrone measurements

NOAA sponsored two Saildrones for the ATOMIC campaign to obtain high quality multiscale air-sea fluxes (Zhang et al., 2019) in two different regimes. Both were launched from Bridgetown, Barbados on Jan. 12, 2020. Saildrone SD1063 focused on the large ocean eddies southeast of BCO, where the North Brazil Current Rings propagate northwestward toward Barbados. Saildrone 1064 sampled in Trade Wind Alley along the leg between BCO and NTAS. In addition, Saildrone 1064 coordinated sampling with the *RV Ronald H. Brown*, remote sensing from research aircrafts, NTAS, Wave Gliders, and SWIFTs. Saildrones 1063 and 1064 were equipped to measure near surface ocean temperature and salinity, upper-ocean current profiles (6m-100m), surface air temperature, humidity, pressure, wind direction and speed, wave height and period, short- and long-wave radiation, and cloud images (Table 10). This system enabled calculation of the bulk latent heat flux and direct turbulent fluxes of momentum and sensible heat. Six thermistors were strapped on the keel to measure the surface layer stratification. Onboard data processing included averaging and motion correction. One-minute averages (5-minute average for ADCP current) were telemetered in real time, while high resolution data were downloaded after the Saildrones returned to U.S. During the 1-month ATOMIC intensive observation period of Jan. 12 to Feb. 12, Saildrone 1064 continuously measured air-sea interaction processes between BCO and NTAS and sailed 1777 nautical miles. After ATOMIC, the Saildrones continued their observations until July 16 and then sailed back to the U.S. arriving in Newport, RI on August 30, 2020.

Three additional Saildrones were piloted by a NASA-funded effort. These data and their details are posted at https://podaac.jpl.nasa.gov/dataset/SAILDRONE_ATOMIC, https://doi.org/10.5067/SDRON-ATOM0.

2.9. RAAVEN UAS measurements

The University of Colorado operated a small remotely-piloted aircraft system (RAAVEN) from Morgan Lewis Beach on the northeastern shore of Barbados between Jan. 24 and Feb. 16. The miniFlux payload flew onboard the RAAVEN UAS (de Boer et al., 2021). Flights conducted during this campaign targeted the thermodynamic and kinematic structure of the lower atmosphere, with sampling occurring between the surface and 1 km altitude. The vast majority of the flights were focused on the sub-cloud layer, with extended sampling conducted at cloud base and a sequence of set altitudes within the sub-cloud layer. Included in these flights were regular sampling intervals at 20 m above the ocean surface to collect information on turbulent surface fluxes of heat and momentum. Most flights were conducted in the near-coastal zone between 0 and 2 km from the coastline. MiniFlux sensors included a multihole pressure probe (MHP); fine-wire array; IR thermometers; pressure, temperature and humidity sensors similar to those used in radiosondes and dropsondes; redundant pressure, temperature, and humidity probes; and an inertial navigation system.

600 **Table 10**. Instrumentation onboard the NOAA sponsored Saildrones. 1-minute averages (5-minute average for
601 ADCP current) were telemetered in real time except where noted below. Final data products are 1-min averages of
602 high resolution raw data.

Instrument	Measured quantity	Height (+) Depth (-) (m)	Raw sampling interval
Gill WindMaster 1590-PK	Wind velocity (true and relative), GPS position, COG, SOG, magnetic heading, temp, pressure, pitch and roll	+5.2	0.1 sec
Rotronic Hygroclip 2	Air temperature, relative humidity	+2.3	1 sec
SPN1 Delta-T Sunshine pyranometer	Short wave radiation	+2.8	0.2 sec
Eppley Precision Infrared Radiometer (PIR)	Long wave radiation, temperature	+0.8	1 sec
VectorNav VN300 DualGPS aided IMU (Wing)	GPS position, COG, SOG, magnetic heading, pitch and roll (motion correction for WindMaster and SPN1)	+2.575	0.05 sec
VectorNav VN300 DualGPS aided IMU (Hull)	Wave height and wave period and motion correction for ADCP currents	+0.34	0.05 sec
LICOR LI-192SA	Photosynthetically Active Radiation (PAR)	+2.6	1 sec
WET Labs ECO-Fluorometer	Chlorophyll-a (experimental)	-0.5	1 sec
RBR C.T.ODO.chl-a	Conductivity, temperature, dissolved O2, Chl-a (experimental)	-0.53	Inductive CTD
Teledyne RDI Workhorse 300kHz ADCP	Ocean current profiles	-6 to -100	1 sec, 5 min avg. sent via telemetry
Heitronics CT15.10	Skin seawater temperature (experimental)	0	1 sec
Vaisala PTB 210	Barometric pressure	+0.2	1 sec
4 Cameras	Cloud image	Upward, sideways, downward	Every 5 min, telemetered every 30 min
Seabird SBE57 temperature loggers	Temperature	-0.3, -0.6, - 0.9, -1.2, -1.4, -1.7	1 sec, 1 min avg. not telemetered
Seabird SBE37 CTD+DO	Conductivity, temperature, depth, dissolved O2	-0.5	Pumped, burst sampled 10 sec for 1min/5 min

603

604

605 **2.10. SVPS drifter measurements**

606

607 Though not deployed from the *R/V Ronald H. Brown*, the ATOMIC field campaign and its archive also includes a

608 dataset of 9 SVPS type surface ocean drifters deployed by NOAA AOML (Surface Velocity Program Salinity,

609 (Centurioni et al., 2015;Hormann et al., 2015)). These were deployed from the EUREC[4]A ship *RV L'Atalante* 50 to

610 150 NM from the South American coast, between 6°N and 10°N, the so-called Boulevard de Tourbillons (Eddy

611 Boulevard), where North Brazil Current Rings translate northwestward (Fig. 1b). The purpose of these drifters was

612 to measure air-sea interaction, ocean properties, and atmospheric variability amidst ocean eddies and low-salinity

613 plumes from a Lagrangian perspective. During ATOMIC the SVPS drifters measured air pressure and relative wind

614 at 0.5 m height. They also measured ocean salinity and temperature (0.3, 5, 10 m depth, with a duplicate T sensor at
615 0.3 m), and ocean velocity representative of water located between 11-19 m depth and centered at 15 m. The drifter
616 was equipped with a drogue centered at 15 m in the form of a long vertically-oriented holey sock. The drogue's full
617 extent spanned a depth of 11.34 m to 18.66 m. Therefore, currents calculated from the drifter location are
618 representative of currents between these depths. Bulk wind stress and the bulk drag coefficient were estimated from
619 these data using COARE 3.6. Data records began at different times and locations to sample different ocean features.
620 Four drifters started on Jan. 23, 1 drifter on Jan. 26, 4 drifters on Feb. 2, and 1 drifter on Feb 4. The drifters exited
621 the ATOMIC/EUREC4A region on about Apr. 29, which marks the end of this archived ATOMIC dataset. After
622 this date, data were still being reported from some sensors and can be accessed by contacting the PI (Table 11). The
623 drifter sensors sampled every 90 sec and then computed averages over 30 min. The averaged data were transmitted
624 to land via satellite telemetry. The position and time data were instantaneous every 30 min. Ten total drifters were
625 deployed but GPS did not work on one so that dataset is not posted.
626
627 **2.11. BACO aerosol measurements**
628
629 Size resolved cloud condensation nuclei (CCN) number concentrations were measured with a custom-made
630 differential mobility analyzer (DMA) for size selection connected to a Droplet Measurement Technologies (DMT)
631 CCNC-100 and a GRIMM 5.412 CPC. Aerosol number size distributions were made with a Scanning Mobility
632 Particle Sizer (SMPS) (GRIMM 5.420) with a diameter range of 0.10 to 1.094 μm. Measurements were made from
633 an isokinetic aerosol inlet located at roughly 47 m.a.s.l.
634
635 **2.12. BCO measurements**
636
637 BCO is at a height of 25 m.a.s.l. Meteorological sensors (Vaisala WXT-520) were mounted at 4 m.a.g.l. BCO
638 launched 182 radiosondes. Data from the sondes were merged into the EUREC[4]A sounding network (Stephan et al.,
639 2020). A Lufft ceilometer CHN 15k NIMBUS was used for the determination of cloud base height.
640
641 **3. Overview of meteorological and surface seawater conditions sampled**
642
643 During ATOMIC, the *RV Ronald H. Brown* primarily operated in Trade Wind Alley, north of 12.5°N between
644 ~56°W and NTAS (Fig. 1a). During the boreal winter, near-surface winds from the northeast carry air masses from
645 NTAS to BCO in about 1.5 d. Positioning the *RV Ronald H. Brown* in Trade Wind Alley allowed for sampling of
646 atmosphere and ocean conditions from the surface in between NTAS and BCO. Winds were fairly steady throughout
647 the cruise with an average speed (10 m) of 8.3 ± 2.1 m sec^{-1} and direction of 70 ± 21° (Fig. 4a). Air temperature (10
648 m) ranged between 22.7 and 27.9°C and averaged 25.7 ± 0.61 °C. RH averaged 71 ± 4.7% (Figure 4b). Radiosondes
649 launched within Trade Wind Alley revealed dryer conditions in the lower and middle troposphere compared to
650 observations made to the south in the Boulevard de Tourbillons which paralleled the coast of South America (Fig.

651 1b). Stephan et al. (2020) attribute the difference to more frequent periods of a deep moist layer and deeper

652 convection to the south.

653

654 Rain rate was measured by three instruments during the cruise located at different places on the ship. Two Parsivel

655 disdrometers were located on the port rail on the O3 deck, an ORG-815 DA optical range gauge was located on the

656 mast tower, and a Vaisala WXT536 was mounted on top of an aerosol sampling van on the O2 deck. Although

657 instruments and locations were not identical, a coherent picture of rain occurrence emerges with frequent events

658

659 **Figure 4.** Time series of bow mast measurements of a) wind speed and direction, b) air temperature and relative
660 humidity all adjusted to 10 m height using the COARE 3.6 bulk model. Also shown are c) rain rate measured with
661 three different instruments, d) dust and elemental carbon mass concentration for particles with aerodynamic
662 diameters less than 10 μm, and e) skin seawater temperature from the sea snake and downwelling longwave
663 radiation.

664

665

666
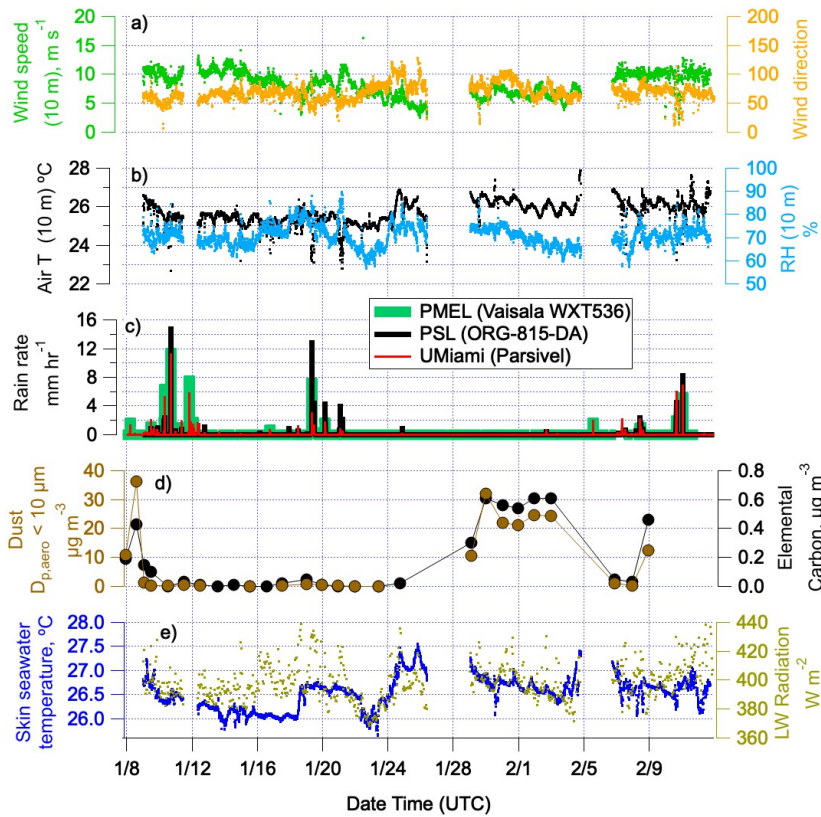
667 between Jan. 9 and 12; Jan. 19 and 21; and Feb. 8, 10, and 11 (Figure 4c). January rain events were associated with a

668 stationary front extending along 20°N from the east into Barbados. February events occurred as an Atlantic ridge

669 progressed eastward inducing strong winds and scattered showers.

670

671 One unique feature of the atmospheric conditions during ATOMIC was the occurrence of high concentrations of

672 dust in the boreal winter. Dust concentrations have long been documented to increase each summer in the Caribbean

673 due to transport from Africa (Prospero and Mayol-Bracero, 2013). A layer of warm, dry air above the marine

674 boundary, known as the Saharan Air Layer (SAL), extends from Africa to North America during the summer which

675 leads to relatively long aerosol residence times and efficient transport of dust between the two continents (Petit et

676 al., 2005;Carlson and Prospero, 1972). Factors contributing to dust transport to the Caribbean during the winter are

677 not as well understood but have been shown to correlate with the southward movement of the Intertropical

678 Convergence Zone (ITCZ) which affects near-surface northeasterly winds over North Africa (Doherty et al., 2012).

679 As a result, the SAL occurs at lower altitudes and more southern latitudes in the winter (Tsamalis et al., 2013;Liu et

680 al., 2012).

681

682 Filter measurements of particulate Al, Si, Ca, Fe, and Ti onboard the *RV Ronald H. Brown* were used to derive dust

683 concentrations (Malm et al., 1994). As shown in Fig. 4d, elevated dust concentrations were observed at the

684 beginning of Leg 1 (Jan 8 00:00 to Jan. 9 12:00) and two more times during Leg 2 (Jan. 29 12:00 to Feb. 3 19:00

685 and Feb. 9 00:00 to Feb. 11 12:00). Dust concentrations were still elevated when aerosol sampling was halted on

686 Feb. 3 and Feb. 11. Elemental carbon (EC) concentrations were enhanced during these same periods indicating

687 transport of biomass burning along with the dust. The NASA Fire Information for Resource Management System

688 (FIRMS) satellite product indicated a wide swath of fires over North Africa during January and February of 2020

689 (https://earthdata.nasa.gov/earth-observation-data/near-real-time/firms).

690

691 The ATOMIC study area was characterized by warmer skin seawater temperatures nearer to Barbados (west of

692 ~55°W) due, in part, to the North Brazil Current (NBC) that transports South Atlantic warm water along the coast of

693 Brazil and into the northern hemisphere, separating from the coast around 6° to 8°N. Occasionally the NBC curves

694 back on itself and pinches off warm eddies that move further north and into the Caribbean Sea (Fratantoni and

695 Glickson, 2002). The coolest skin seawater temperatures were encountered in the vicinity of the NTAS and MOVE

696 operations on the most northeastern portion of the cruise track between Jan. 12 and 16 (Fig. 1a and Fig. 4e). A

697 second period of low skin seawater temperatures coincided with sustained relatively low longwave downwelling

698 radiation on Jan. 22 and 23 (Fig. 4e) although causes of the low temperatures have yet to be determined.

699

700 **4. Inter-platform data comparisons**

701

702 Times when the *RV Ronald H. Brown* was in close proximity to or upwind of other sampling platforms are listed in

703 Table 3. These periods provide the potential for inter-platform comparisons for data quality checks or scientific

704 purposes. Inter-platform comparisons reported here include 1) NTAS moorings and the ship (seawater and

705 atmospheric parameters), 2) Saildrone 1064 and the ship (seawater and atmospheric parameters), 3) BCO and the

706 ship (atmospheric parameters), 4) BACO and the ship (aerosol properties), and 5) BCO, the ship, and RAAVEN

707 UAS (cloud base height). These comparisons were done to evaluate consistencies in the measurements. Resolving

708 identified inconsistencies will be the subject of future research.

709

4.1. Comparison of seawater parameters

4.1.1. Onboard RHB. No significant offsets or biases were found among the independently calibrated subsurface temperature measurements onboard *RV Ronald H. Brown*. Measurements from the ship's CTD, uCTD, PSL sea snake, and ship's underway thermosalinograph and thermistor were similar. After correcting for a small bias found in the uCTD salinity, no significant difference was found among the different salinity measurements recorded.

4.1.2. NTAS – RHB. Four CTD casts with the ship's rosette were conducted to compare to the NTAS moorings' upper ocean measurements between Jan. 12 and 15. The ship was 3 NM southwest of the NTAS-18 mooring anchor on Jan. 12 and 13 and 3.8 NM northwest of the NTAS-17 mooring anchor on Jan. 15 (Table 3 and Fig. 5a). With an anchor radius watch circle of ~ 2 NM for each buoy, the ship and buoys were within 0.25 to 3 NM of each other. NTAS measurements of temperature and salinity at 5 depths (10, 25, 40, 55, and 70 m) are overlaid onto data from the ship's CTD in Figure 5. Absolute differences (NTAS – RHB) in temperature are less than 0.1°C for all depths of the three casts conducted on Jan. 12 and 13 except for the last cast during that period (Fig. 5j). For the most part, the salinity comparisons show good agreement for the Jan. 12 and 13 casts with absolute differences at depths between 10 and 40 m being less than 0.03 (Fig.5 k). Exceptions occurred at lower depths due to strong vertical gradients.

The comparison from Jan. 15 shows significant differences for both temperature (Fig. 5j) and salinity (Fig. 5k) likely due to horizontal gradients. Satellite derived sea surface salinity and SST for this day indicate that NTAS and the ship were located in a frontal region with the ship in warmer and saltier surface water to the north of NTAS. The sign of the absolute differences (NTAS – RHB) in temperature and salinity varied with depth. The ship's ADCP revealed vertical structure in the currents consistent with the sign of observed absolute differences at the surface versus lower depths.

4.2. Comparison of atmospheric parameters

4.2.1. NTAS – RHB

Atmospheric parameters (temperature, relative humidity, specific humidity, wind speed, pressure, rain rate, and longwave downwelling radiation) measured onboard the NTAS buoys and the *RV Ronald H. Brown* were compared when the platforms were within 3 NM of each other between Jan. 10 and 15 (Table 3). Measurements from NTAS-17 and NTAS-18 were combined into one data set for the comparison. Based on 1-hr averaged data, 59 samples were available for comparison.

Wind speed, temperature, and specific humidity from both platforms were adjusted to a height of 10 m. Absolute differences (NTAS – RHB) were positive for temperature (Fig. 6a), RH (Fig. 6b), specific humidity (Fig. 6c), and wind direction (Fig. 6d). These differences, however, were within either reported accuracies of the instrumentation

747   or within the range reported for a previous 24-hr *RV Ronald H. Brown* – Stratus 4 buoy comparison (Colbo and

748   Weller, 2009). Absolute differences (NTAS – RHB) were negative for wind speed, pressure, rain rate, and longwave

749   downwelling radiation although all differences were within accuracies of the instrumentation or within the range

750   reported by Colbo and Weller (2009).

751

752

753

754

755 **Figure 5.** Comparison of upper ocean measured parameters from the NTAS 18 mooring and the *RV Ronald H.*
756 *Brown* on Jan. 12, 13, and 15 with a) location of NTAS-18 mooring anchor. The NTAS buoys were about 2 NM
757 downwind (SW) of the anchor so the CTD and mooring measurements were within 0.5 to 3 NM of each other. Also
758 shown are b – e) temperature, f – i) salinity, and j – k) absolute differences and root mean square differences (rmsd)
759 for temperature and salinity, respectively. Number of samples = 4.
760

761
762
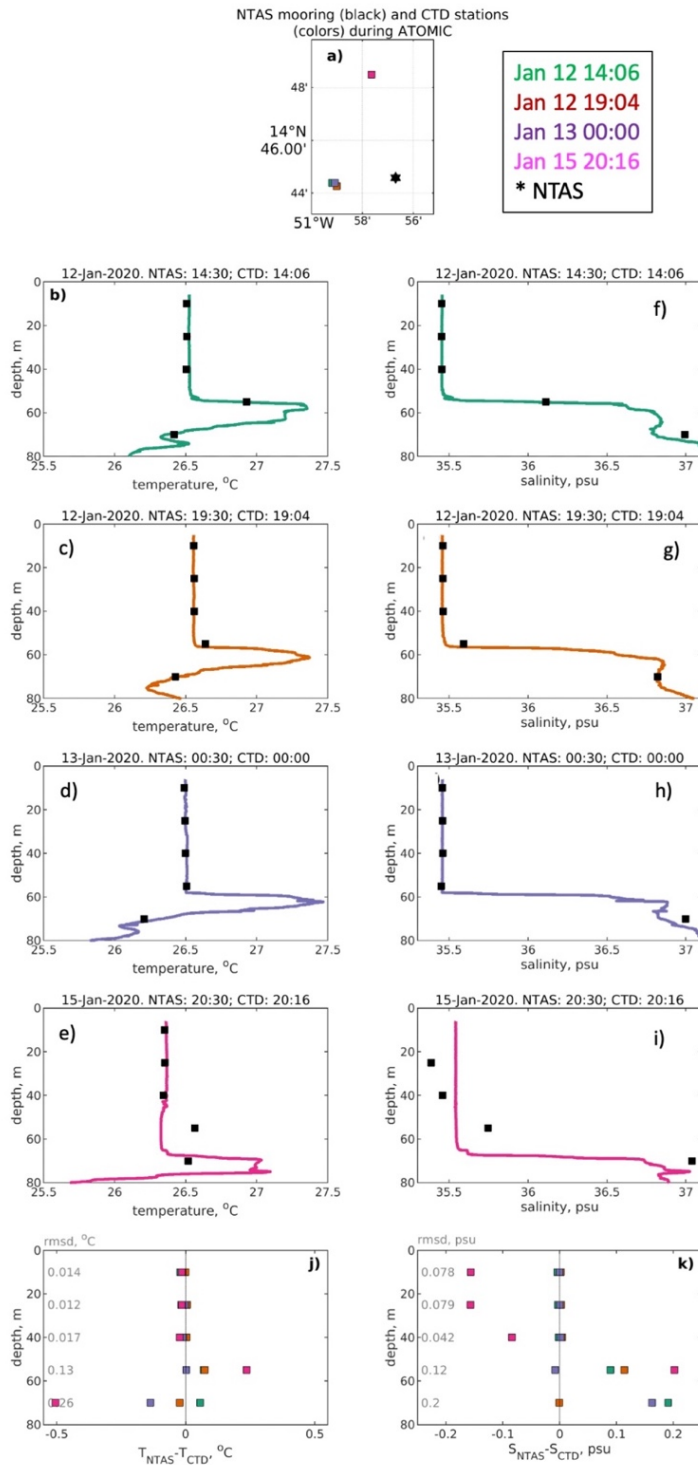
763 **Figure 6.** Comparison of meteorological parameters measured onboard the NTAS buoy and the *RV Ronald H.*
764 *Brown* (RHB) when the platforms were between 0.25 and 3 NM apart between Jan. 10 and Jan. 15 including a)
765 atmospheric temperature (10 m), b) relative humidity (10 m), c) specific humidity (10 m), d) wind direction, e) wind
766 speed (10 m), f) atmospheric pressure (10 m), g) rain rate, and h) longwave downwelling radiation. The averaged of
767 absolute differences (NTAS – RHB) and root mean square differences (rmsd) are reported in the inset table. Number
768 of samples based on 1 hr averaged data = 59.
769
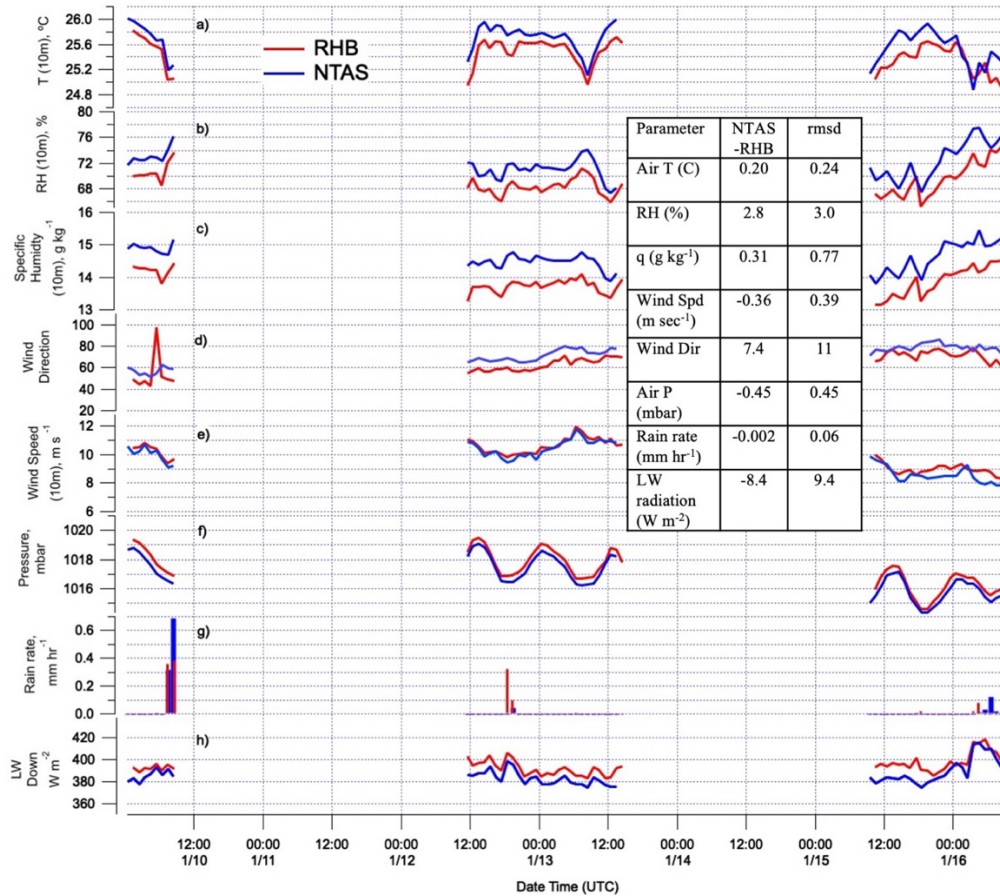
770
771
772 4.2.2. BCO – RHB
773
774 The Barbados Cloud Observatory (BCO) is located at Deebles Point on the eastern coast of Barbados. Atmospheric
775 parameters (temperature, RH, wind direction and speed, pressure, and rain rate) were compared between BCO and
776 the ship during the period the ship was 20 NM east and upwind of the observatory (Jan. 24 18:20 to Jan. 25 23:40)
777 (Table 3). BCO meteorological sensors were located at 30 m.a.s.l. and were not adjusted to a height of 10 m due to
778 uncertainties in adjusting overland measurements (BC0) with surface fluxes from the *RV Ronald H. Brown.* Based
779 on 10-min averaged data, 177 samples were available for comparison.
780
781 The average of the absolute difference (BCO – RHB) in temperature over the entire period was larger than
782 instrumental accuracies (Fig. 7a). The largest difference was observed after 12:00 UTC (08:00 local) indicating

783   relatively more warming of the sensor and/or atmosphere at BCO due to diurnal heating of the land surface. Even

784   with differences in temperature, RH values from the two platforms agreed well with the exception of the end of the

785   period. The ship observed an abrupt change in temperature and RH on Jan. 25 at 19:30 (Fig. 7a,b) suggesting that

786   the platforms were in different air masses. Wind direction agreed well between platforms (Fig. 7c) but the average

787   of the absolute differences (BCO – RHB) in wind speed (Fig. 7d) and pressure (Fig. 7e) were larger than

788   instrumental uncertainties. One rain event occurred during the comparison. It was observed on Jan. 24 on the ship

789   and 30 minutes later at BCO with observed rain rates of 1.2 and 3.5 mm hr^{-1}, respectively (Fig. 7f).

790

791   **Figure 7.** Meteorological parameters measured during the *RV Ronald H. Brown* (RHB) and the Barbados Cloud
792   Observatory (BCO) comparison (Jan. 24 18:20 to Jan. 25 23:40) when RHB was 20 NM due east of BCO.
793   Parameters include a) atmospheric temperature, b) relative humidity (RH), wind direction, wind speed, atmospheric
794   pressure, and rain rate. The average of the absolute differences (BCO – RHB) and root mean square differences
795   (rmsd) are reported in the inset table. BCO meteorological sensors were located at 30 m.a.s.l. and were not adjusted
796   to a height of 10 m. Number of samples based on 10 minute averaged data = 177.

797

Parameter	BCO – RHB	rmsd
Air T (C)	0.53	0.74
RH (%)	-0.39	3.4
Wind Dir	5.5	14
Wind Spd (m sec^{-1})	-2.0	2.3
Air P (mbar)	-2.6	2.6
Rain rate (mm hr^{-1})	2.3*	

*n = 1 (Jan. 20 event with BCO shifted 0.5 hr earlier)

798

799

800

801   4.2.3. SD1064 – RHB

802
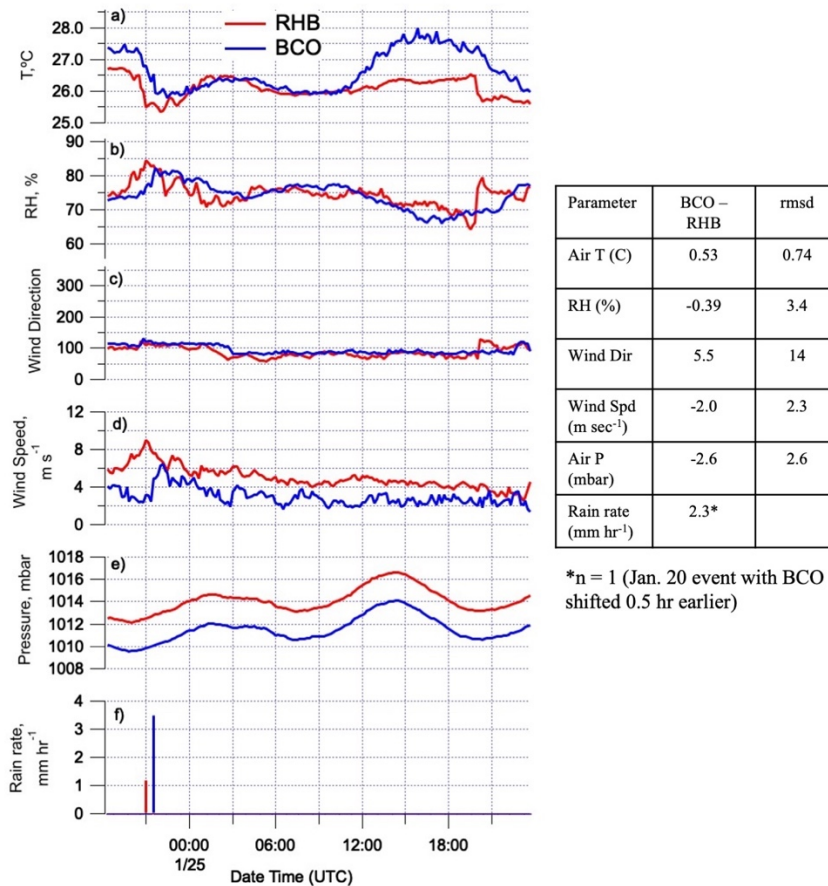
803   Saildrone 1064 and the *RV Ronald H. Brown* were within 0.7 to 3.6 NM of each other between Feb. 8 and 10.

804   Based on 10 min averaged data, 663 samples were available for the comparison. Air temperature, RH, and wind

805   speed adjusted to 10 m were used for the comparison. Skin seawater temperature was measured at a depth of 0.05 m

806   on the Saildrone and from the ship's Sea Snake. On average, skin seawater temperature agreed within 0.01°C,

807   atmospheric temperature within 0.12 °C, and RH within 1.9%. – all within the uncertainty of the measurements or

808   within the agreement observed between the NTAS buoy and the ship (see Sect. 4.2.1.) (Fig. 8a, b, c). At the end of

809   the comparison, ship measured seawater temperature at 0.05 m decreased, atmospheric temperature decreased, and

810   RH increased while Saildrone observed parameters remained steady even though the platforms were within 0.8 NM

811   of each other. These differences indicate the fine scale nature of structural differences in surface oceanic and lower

812   atmospheric conditions.

813

814   On average, agreement for wind direction and wind speed was not within instrumental uncertainties or the

815   agreement observed between the NTAS buoy and the ship due to spikes in the ship's measurements not observed by

816   the Saildrone (Fig. 8d, e). Atmospheric pressure agreed well with an absolute difference (SD0164 – RHB) of -0.27

817   mbar (Fig. 8f). The absolute difference in downward long wave radiation (SD0164 – RHB) was 4.4 W m^{-2},

818   indicating a systemic offset (Fig. 8g).

819

820

821 **Figure 8.** Comparison of parameters measured onboard Saildrone 1064 (SD1064) and *RV Ronald. H. Brown* (RHB)
822 when the platforms were within 0.7 to 3.6 NM of each other between Feb. 8 and 10. Parameters include a) SST (SD
823 at -0.05 m and RHB Sea Snake), b) air temperature (10 m), c) RH (10 m), d) wind direction, e) wind speed (10 m),
824 f) atmospheric pressure (10 m), and g) longwave downwelling radiation. Absolute differences (SD1064 – RHB) and
825 root mean square differences (rmsd) are reported in the inset table. Number of samples based on 10 min averaged
826 data = 663.

827
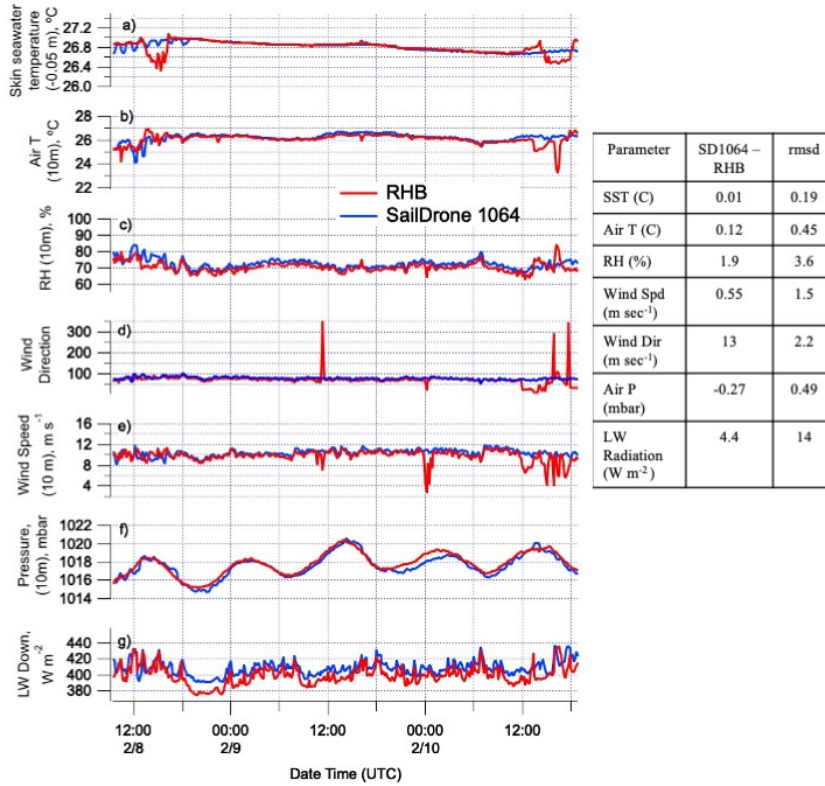
828   **4.3. Comparison of aerosol and cloud parameters**

829

830   4.3.1. BACO – RHB – aerosol parameters

831

832   The Barbados Atmospheric Chemistry Observatory (BACO) is located at Ragged Point, 400 m across a cove from

833   BCO. Total particle number concentration (CN), cloud condensation nuclei (CCN) concentration at 0.4%

834   supersaturation, and particle number size distributions were compared between BACO and the ship when the ship

835   was 20 NM east and upwind of BACO (Jan. 24 18:20 to Jan. 25 23:40) (Table 3). Details on the *RV Ronald H.*

836   *Brown* aerosol measurements are shown in Table 5 and details on CCN calibration and measurements are provided

837   in Quinn et al. (2019). Details on BACO CCN calibrations and measurements are provided in Pöhlker et al. (2018).

838

839   CN and CCN concentrations are shown in Fig. 9 from the time when BACO measurements began (Jan. 22 00:16) to

840   when the ship's measurements ended (Feb. 9 20:20). Based on CN concentrations below 300 cm^{-3}, both platforms

841   encountered clean marine conditions until ~Jan. 29 at 12:00. Subsequent enhanced concentrations of both CN and

842   CCN correspond to periods when dust and biomass burning reached the study area after transport from Africa (Fig.

843   4d) as observed in related earlier studies (Wex et al., 2016). The coherence of CN and CCN between the platforms,

844   even when separated by 4 degrees of longitude, indicates a broadscale dust event.

845

846   **Figure 9.** Aerosol parameters measured onboard the *RV Ronald H. Brown* (RHB) and at Barbados Atmospheric
847   Chemistry Observatory (BACO) for the period of overlapping measurements. The rectangle indicates the
848   comparison period (Jan. 24 18:20 to Jan. 25 23:40) when RHB was 20 NM due east of BACO. Parameters include a)
849   total particle number condensation (CN) and b) cloud condensation nuclei concentration (CCN) measured at 0.4%
850   supersaturation. The average of the absolute differences (BACO – RHB) and root mean square differences (rmsd)
851   for the comparison period are reported in the inset table. Number of samples = 5.

852
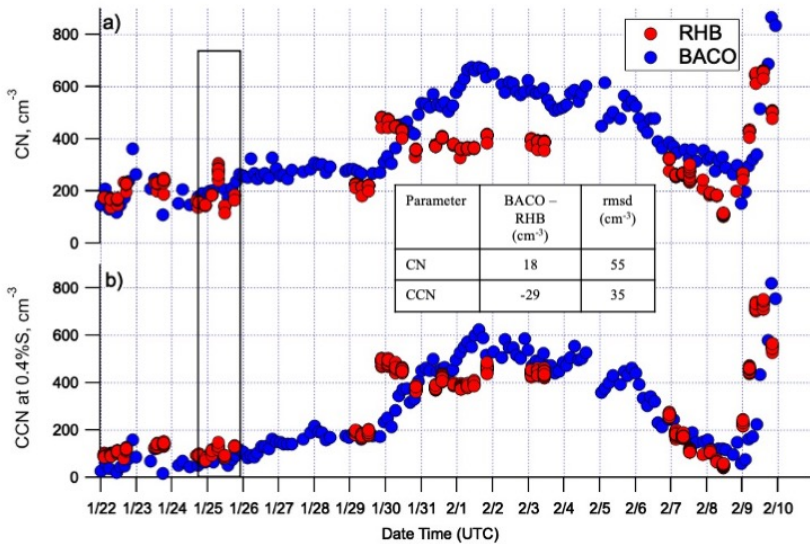
853   The comparison when the ship was 20 NM upwind of BACO is indicated by the rectangle in Fig. 9. CCN

854   concentrations were compared at a single supersaturation (S = 0.4%) which limited the number of samples to 5. The

855   absolute difference (BACO – RHB) was 18 cm^{-3} for CN, which is less than 10% of the average CN concentration

856   during the comparison period and less than measurement uncertainties (Rose et al., 2008) (Fig. 9a). The difference

857   for CCN was -29 cm^{-3} indicating the ship observed more CCN at S = 0.4% than BACO (Fig. 9b). However, this

858   difference is within the combined uncertainty of 30% for mono- and polydisperse CCN measurements.

859

860   Shipboard and BACO size distributions averaged over the length of the comparison were bimodal with Aitken

861   modal diameters of ~40 nm for both the ship and BACO and 130 and 170 nm for the accumulation mode for the

862   ship and BACO, respectively (Fig. 10). Differences in magnitude could be due to instrumental issues or local

863   aerosol sources at BACO.

864

865   **Figure 10.** Comparison of aerosol number size distribution measured onboard the *RV Ronald H. Brown* (RHB) and
866   at the Barbados Atmospheric Chemistry Observatory (BACO) during the comparison period (Jan. 24 18:20 – Jan. 25
867   23:40) when RHB was 20 NM to the east of BACO.

868

869

870
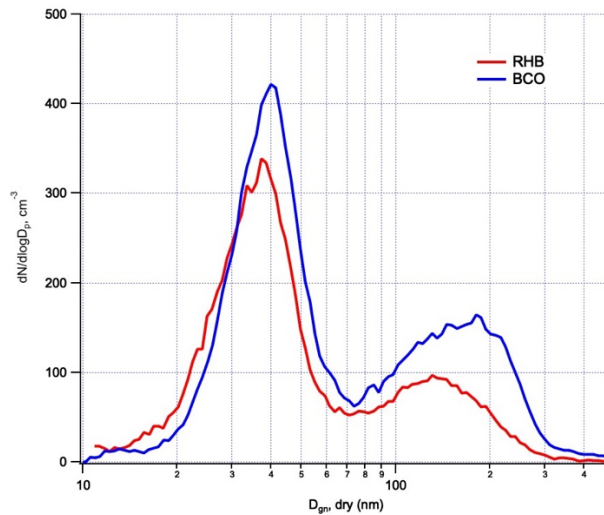
871   4.3.2. BCO – RHB – cloud base height

872

873   Cloud base height (CBH) was derived from three different measurements onboard the *RV Ronald H. Brown* – LCL

874   calculated from the stitched together RHB – BCO radiosonde record (equation 1), the ceilometer, and the microDop

875   lidar (Fig. 11a). Fifth and 10th percentile values of the lowest cloud scattered return were averaged over 10 min

876   intervals of the ceilometer and lidar data, respectively. The choice of percentile levels was tested to reduce inclusion

877   of scattering at the surface made by rain and scattering aloft from horizontally-sheared cloud edges. Higher altitude

878   ceilometer and lidar values that remain in this time series are not representative of cloud base due to the presence

879   and scattering by sheared edges or detrained portions of clouds that are separated horizontally from the locations of

880   cloud base. Dilution of surface parcels with drier air could also contribute to rising heights of the cloud base. Lowest

881   values from both the ceilometer and lidar track well with the LCL values derived from the radiosondes.

882   **Figure 11.** Comparison of Cloud Base Height (CBH) for a) legs 1 and 2 onboard *RV Ronald H. Brown* (RHB) based
883   on LCL calculated from the stitched together RHB – BCO radiosonde record (equation 1), the ceilometer, and the
884   Doppler lidar and b) for the RHB – BCO comparison period (Jan. 24 18:20 – Jan. 25 23:40) based on the BCO
885   ceilometer, LCL from BCO radiosondes, the RHB ceilometer and microDop lidar, and the RAAVEN UAS flown
886   from Morgan Lewis (30 km north of BCO). Locations of the RAAVEN launch site, BCO, and RHB are shown in c).
887   The average of the absolute differences and root mean square differences (rmds) are shown in the table inset relative
888   to the RHB lidar-derived CBH. N indicates number of samples used in the comparison. *rmsd for RHB ceilometer –
889   RHB microDop lidar with CBH greater than 1000 m removed from comparison.

890

891

892
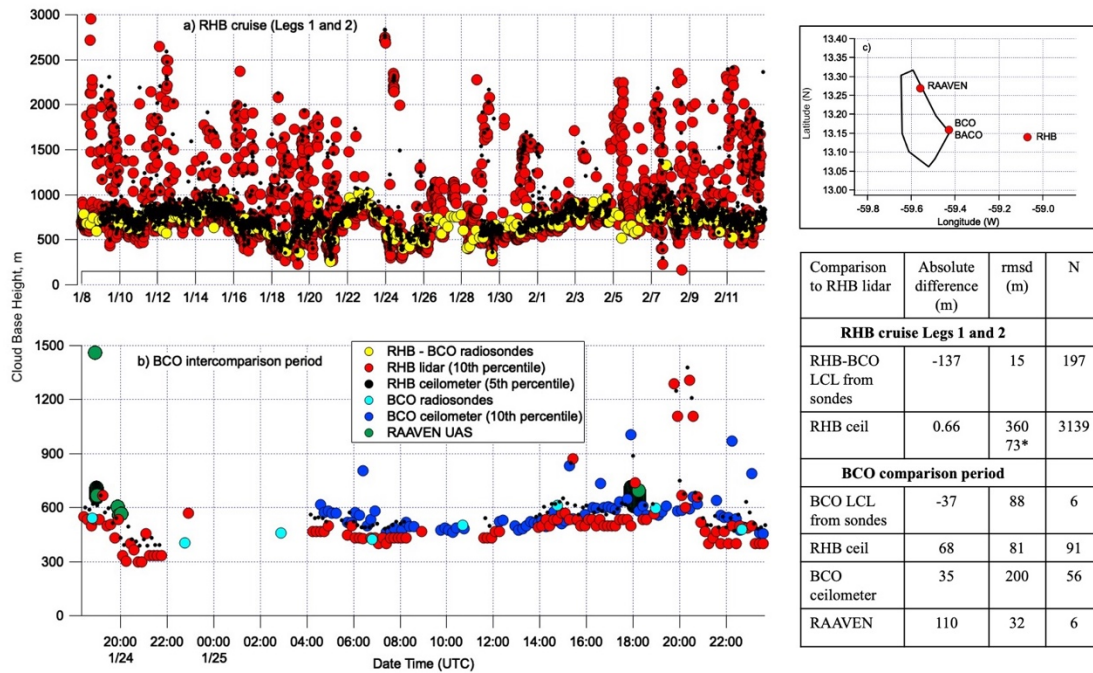
893   On average, the absolute difference between the LCL and lidar values (RHB-BCO LCL – RHB lidar) is -137 m due

894   to lidar scattering off of slightly higher altitude clouds. On average, the absolute difference between the RHB

895   ceilometer and microDop lidar (RHB ceilometer – RHB lidar) is 0.66 m indicating good agreement while the rmsd

896   value of 360 m reveals larger point to point differences. If CBHs from the ship's ceilometer and microDop lidar are

897   limited to values less than 1000 m, rmsd decreases to 73 m.

898

899   For the BCO comparison period (Jan. 24 18:20 – Jan. 25 23:40), CBHs were compared from the ship's ceilometer

900   and microDop lidar, BCO's ceilometer and LCLs from radiosondes, and the RAAVEN UAS miniFlux payload (Fig.

901   11b). The RAAVEN UAS flew from the eastern side of Barbados, 30 km north of BCO. Locations of the RAAVEN

902   launch site, BCO, and ship during the comparison are shown in Fig. 11c. Absolute differences in average values

903   between the BCO ceilometer and RHB microDop lidar (BCO ceilometer – RHB microDop lidar) and BCO LCLs

904   and RHB microDop lidar (BCO LCL – RHB microDop lidar) are around 35 m or 7% of the average sonde-derived

905   CBH. The absolute difference in average values between the RHB ceilometer and RHB microDop lidar (RHB

906   ceilometer – RHB microDop lidar) is slightly higher at 68 m. RAAVEN values are slightly higher with an absolute

907   difference (RAAVEN miniFlux – RHB microDop lidar) of 110 m. Differences could be related to finer-scale

908   horizontal and vertical variability in boundary layer structure not readily-resolved by the measurements.

909

910   **5. Data availability**

911

912   All ATOMIC data sets discussed herein are publicly available at the NOAA PSL ATOMIC ftp server

913   (ftp://ftp2.psl.noaa.gov/Projects/ATOMIC/data/) and NOAA's National Center for Environmental Information

914   (https://www.ncei.noaa.gov/access/metadata/landing-page/bin/iso?id=gov.noaa.nodc:ATOMIC-2020). Point of

915   contact information, links and DOIS for the individual data sets are provided in Table 11. The data will be

916   permanently and publicly available on the PSL ftp server and NCEI.

917

918   A readme file (README_ATOMIC_DATA.pdf) is available at ftp://ftp2.psl.noaa.gov/Projects/ATOMIC/data/

919   which describes the file structure of the ATOMIC folder and the content of the single files.

920

921   All of the datasets included in the discussion have been quality-controlled based on procedures implemented by the

922   individual research teams. Versioning also is based on protocols put in place by individual research teams. Details

923   can be found in the references listed in Table 11. Data are CF compliant. File name structure is:

924

925   <campaign_id>_<project_id>_<platform_id>_<instrument_id>_<variable_id>_<time_id>_<version_id>.nc.

926

927   An example for data collected from the ceilometer on the *RV Ronald H. Brown* is as follows. The name of the data

928   and link are:

929

930   EUREC4A_ATOMIC_RonBrown_Ceilometer_10min_20200109_20200212_v1.0.nc.

931

932   Metadata are embedded in the individual .nc files for each data set.

933

934

935 **Table 11**. Summary of data sets, links and DOIs for the data sets, point of contact information, and references for
936 data collected onboard the *RV Ronald H. Brown*, NTAS, Wave Gliders, SWIFTs, NOAA and NASA operated
937 Saildrones, and RAAVEN UAS during ATOMIC. Links in the table are for the ftp server
938 (ftp://ftp2.psl.noaa.gov/Projects/ATOMIC/data/) and NOAA's National Center for Environmental Information
939 (https://www.ncei.noaa.gov/access/metadata/landing-page/bin/iso?id=gov.noaa.nodc:ATOMIC-2020). The data will
940 be permanently and publicly available on the PSL ftp server, and NCEI.
941

Platform	Data set	Data Links	Point of Contact	Reference
All	ATOMIC	ftp://ftp2.psl.noaa.gov/Projects/ATOMIC/data/ https://www.ncei.noaa.gov/access/metadata/landing-page/bin/iso?id=gov.noaa.nodc:ATOMIC-2020	elizabeth.thompson@noaa.gov	Zuidema (2021)
RHB	Air-sea fluxes, ship navigation/location information, meteorological parameters, solar and infrared radiation, rain rate, subskin seawater T, skin seawater T (NOAA PSL)	ftp://ftp2.psl.noaa.gov/Projects/ATOMIC/data/rhb/met_sea_flux_nav/ https://doi.org/10.25921/etxb-ht19	elizabeth.thompson@noaa.gov	Fairall et al. (1997);Fairall et al. (2003);Edson et al. (2013)
	ROSR skin seawater T (NOAA PSL)	ftp://ftp2.psl.noaa.gov/Projects/ATOMIC/data/rhb/ROSR/ https://doi.org/10.25921/nwx9-rd07	elizabeth.thompson@noaa.gov	
	Ceilometer (NOAA PSL)	ftp://ftp2.psl.noaa.gov/Projects/ATOMIC/data/rhb/ceilometer/ https://doi.org/10.25921/jbz6-e918	elizabeth.thompson@noaa.gov	
	Disdrometer (rain rate, drop number, equivalent radar reflectivity) (U Miami)	ftp://ftp2.psl.noaa.gov/Projects/ATOMIC/data/rhb/disdrometer/ https://doi.org/10.25921/pfgy-7530	pzuidema@rsmas.miami.edu	(Löffler-Mang and Joss, 2000)
	W-band radar (U Miami in partnership with NOAA PSL)	ftp://ftp2.psl.noaa.gov/Projects/ATOMIC/data/rhb/W-band-radar/ https://doi.org/10.25921/44cy-kr53	pzuidema@rsmas.miami.edu elizabeth.thompson@noaa.gov	
	Sky camera (U Miami)	https://www.dropbox.com/sh/zejurecda70bilq/AABlLWgrEv1MDZ07yIE5TgWWa?dl=0	pzuidema@rsmas.miami.edu	
	M-AERI skin seawater T, air humidity and temperature (U Miami)	ftp://ftp2.psl.noaa.gov/Projects/ATOMIC/data/rhb/M-AERI/ https://doi.org/10.25921/db6z-z646	pzuidema@rsmas.miami.edu gszczodrak@rsmas.miami.edu	Szczodrak et al. (2007)
	Doppler lidar (NOAA CSL)	ftp://ftp2.psl.noaa.gov/Projects/ATOMIC/data/rhb/doppler_lidar/ https://doi.org/10.25921/74pc-me66	alan.brewer@noaa.gov	Schroeder et al. (2020)
	Picarro water vapor isotopes (OSU/NCAR)	ftp://ftp2.psl.noaa.gov/Projects/ATOMIC/data/rhb/Picarro/ https://doi.org/10.25921/s76r-1n85	david.noone@auckland.ac.nz	
	Picarro seawater isotopes	ftp://ftp2.psl.noaa.gov/Projects/ATOMIC/data/rhb/seawater_isotopes/	david.noone@auckland.ac.nz	
	Meteorological and aerosol properties (NOAA PMEL)	ftp://ftp2.psl.noaa.gov/Projects/ATOMIC/data/rhb/atmos-chem/ https://doi.org/10.25921/yf54-2c81	derek.coffman@noaa.gov	Bates et al. (2002)
	Radiosondes (OSU)	https://doi.org/10.25326/62	simon.deszoeke@oregonstate.edu	Stephan et al. (2020)
	Underway CTD, uCTD (APL-UW)	ftp://ftp2.psl.noaa.gov/Projects/ATOMIC/data/rhb/UCTD/ https://doi.org/10.25921/nsmv-0c33	kdrushka@apl.uw.edu	Mojica and Gaube (2020)
	Ship rosette CTD (APL-UW)	ftp://ftp2.psl.noaa.gov/Projects/ATOMIC/data/rhb/CTD/	kdrushka@apl.uw.edu	

		https://doi.org/10.25921/zycs-th03		
	Ship ADCP (APL-UW)	ftp://ftp2.psl.noaa.gov/Projects/ATOMIC/data/rhb/ADCP/ https://doi.org/10.25921/b6wh-zr34	kdrushka@apl.uw.edu	
NTAS mooring	Meteorological parameters, air-sea fluxes, solar and infrared radiation; ocean currents, waves, conductivity, salinity, and temperature (WHOI)	ftp://ftp2.psl.noaa.gov/Projects/ATOMIC/data/NTAS/ https://doi.org/10.25921/er1a-hq72	aplueddemann@whoi.edu	Weller (2018)
Wave Gliders	Air-sea fluxes, meteorological parameters, radiation; ocean currents, turbulence, waves, conductivity, and temperature (APL-UW)	ftp://ftp2.psl.noaa.gov/Projects/ATOMIC/data/wavegliders/ https://doi.org/10.25921/dvys-1f29	jthomson@apl.washington.edu	Thomson and Girton (2017)
SWIFT drifter	Air-sea fluxes, meteorological parameters, radiation; ocean currents, turbulence, waves, conductivity, and temperature (APL-UW)	ftp://ftp2.psl.noaa.gov/Projects/ATOMIC/data/swift_drifters/ https://doi.org/10.25921/s5d7-tc07	jthomson@apl.washington.edu	Thomson et al. (2019)
Saildrones (NOAA)	Air-sea fluxes, meteorological parameters, radiation; ocean currents, waves, conductivity, and temperature (NOAA PMEL)	ftp://ftp2.psl.noaa.gov/Projects/ATOMIC/data/saildrones_noaa/ https://doi.org/10.25921/9km0-f614	dongxiao.zhang@noaa.gov	Zhang et al. (2019)
Saildrones (NASA)	Air-sea fluxes, meteorological parameters, radiation; ocean currents, waves, conductivity, and temperature (NASA)	https://doi.org/10.5067/SDRON-ATOM0	cgentemann@faralloninstitute.org	
SVPS drifters	Meteorological and ocean parameters, wind stress (NOAA AOML)	ftp://ftp2.psl.noaa.gov/Projects/ATOMIC/data/svp-s_drifters/ https://doi.org/10.25921/2pzq-4d52	greg.foltz@noaa.gov	Centurioni et al. (2015);Hormann et al. (2015)
RAAVEN miniFlux	Met parameters (Univ. Colorado)	ftp://ftp2.psl.noaa.gov/Projects/ATOMIC/data/CU-RAAVEN/ https://doi.org/10.25921/jhnd-8e58	gijs.deboer@noaa.gov	de Boer et al. (2021)

942

943

944 As an example, the metadata for Cloud Base Height is:

945

946 long_name: cloud base height

947 standard_name: cloud_base_altitude

948 units: km

949 coverage_content_type: thematicClassification

950 instrument: ceilometer_instrument

951 platform: RonBrown

952 coordinates: time

953 cell_methods: time: point

954 valid_range: 0.0, 7.0

955 actual_range: 0.28, 6.86975

956 _FillValue: -9999.0

957 comment: Computed as the 5th percentile of cloud1, the height of first cloud layer detected, from 15 sec raw data

958 over this time period.

959
960

6. Summary

During ATOMIC, *in situ* and remote sensing measurements of oceanic and atmospheric properties and air-sea fluxes were made from the *RV Ronald H. Brown.* In addition, the NTAS mooring, radiosondes, SWIFTs, and Wave Gliders were deployed. Descriptions of the instrumentation onboard the ship and the deployed assets are provided along with the sampling strategy and day-to-day events. Atmospheric and oceanic conditions encountered during the cruise are described. Also detailed is how to access to all data collected. Comparisons were conducted with the NTAS moorings, Saildrone 1064, BCO, BACO, and the RAAVEN UAS. Data from inter-platform comparisons are presented to assess consistency in data sets. Resolving identified inconsistencies will be the subject of future research. The intention of the paper is to advance widespread use of the data by the ATOMIC and broader research communities.

Author contributions. P.K.Q. prepared the paper with the help of all co-authors. E.T. prepared data sets for archival on the PSL ftp server and at NCEI. D.J.C. prepared data for inclusion in the paper's figures. All authors participated in collecting and analyzing ATOMIC data.

Competing Interests. The authors declare that they have no competing interests.

Acknowledgements. We thank the crew of the *RV Ronald H. Brown* for their enthusiastic help and cooperation throughout the ATOMIC cruise and Dr. Edmund Blades and Peter Sealey for technical support at the BACO site. NOAA's Climate Variability and Predictability Program provided funding under NOAA CVP NA19OAR4310379, GC19-301, and GC19-305. The Joint Institute for the Study of the Atmosphere and Ocean (JISAO) supported this study under NOAA Cooperative Agreement NA15OAR4320063. Additional support was provided by the NOAA's Uncrewed Aircraft Systems (UAS) Program Office, NOAA's Physical Sciences Laboratory, and NOAA AOML's Physical Oceanography Division. The NTAS project is funded by the NOAA's Global Ocean Monitoring and Observing Program (CPO FundRef number 100007298), through the Cooperative Institute for the North Atlantic Region (CINAR) under Cooperative Agreement NA14OAR4320158. We would like to thank Dr. David Farrell of the Caribbean Institute for Meteorology and Hydrology (CIMH) for his assistance with the organization of this campaign and Dr. Sandy Lucas of NOAA's Climate Program Office for her efforts that made ATOMIC and related outreach programs a success. This is PMEL contribution number 5172.

References

Banner, M. L., and Morison, R. P.: Refined source terms in wind wave models with explicit wave breaking prediction. Part I: Model framework and validation against field data, Ocean Modelling, 33, 177 - 189, 2010.

Bates, T. S., Coffman, D. J., Covert, D. S., and Quinn, P. K.: Regional marine boundary layer aerosol size distributions in the Indian, Atlantic and Pacific Oceans: A comparison of INDOEX measurements with ACE-1, ACE-2, and Aerosols99, J. Geophys. Res. Atmos., 107, 10.1029/2001JD001174, 2002.

Bigorre, S. P., and Galbraith, N. R.: Sensor performance and data quality control, in: Observing the Oceans in Real Time, edited by: Venkatesan, R., Tandon, A., D'Asaro, E., and Atmanand, M. A., Springer International, 243 - 261, 2018.

Bolton, D.: The Computation of Equivalent Potential Temperature, Monthly Weather Review, 108, 1046 - 1053, 1980.

Bony, S., Stevens, B., Frierson, D. M. W., Jakob, C., Kageyama, M., Pincus, R., Shepherd, T. G., Sherwood, S. C., Siebesma, A. P., Sobel, A. H., Watanabe, M., and Webb, M. J.: Clouds, circulation, and climate sensitivity, Nature Geosci., 8, 261 - 268, 2015.

Bony, S., Stevens, B., Ament, F., Bigorre, S., Chazette, P., Crewell, S., Delanoe, J., Emanuel, K., Farrell, D., Flamant, C., Gross, S., Hirsch, L., Karstensen, J., Mayer, B., Nuijens, L., Ruppert, J. H., Sandu, I., Siebesma, P., Speich, S., Szczap, F., Totems, J., Vogel, R., Wendisch, M., and Wirth, M.: EUREC4A: A field campaign to elucidate the couplings between clouds, convection and circulation, Surveys in Geophysics, 38, 1529 - 1568, 2017.

Carlson, T. N., and Prospero, J. M.: The large-scale movement of Saharan air outbreaks over the northern equatorial Atlantic, Journal of Applied Meteorology, 11.2, 283 - 297, 1972.

Centurioni, L. R., Hörmann, V., Chao, Y., Reverdin, G., Font, J., and Lee, D.-K.: Sea surface salinity observations with Lagrangian drifters in the tropical North Atlantic during SPURS: Circulation, fluxes, and comparisons with remotely sensed salinity from Aquarius, Oceanography, 28, 96 - 105, 2015.

Colbo, K., and Weller, R. A.: Accuracy of the IMET Sensor Package in the Subtropics, J Atmos Ocean Tech, 26, 1867 - 1890, 2009.

de Boer, G., Calmer, R., Cox, C. J., Borenstein, S., Rhodes, M., Choate, C., Hamilton, J., Argrow, B., and Intrieri, J.: Measurements from the University of Colorado RAAVEN Remotely-Piloted Aircraft System during ATOMIC, Earth System Science Data, in preparation, 2021.

Doherty, O. M., Riemer, N., and Hameed, S.: Control of Saharan mineral dust transport to Barbados in winter by the Intertropical Convergence Zone over West Africa, J. Geophys. Res. Atmos., 117, 10.1029/2012JD017767, 2012.

Edson, J. B., Jampana, V., Weller, R. A., Bigorre, S., Plueddemann, A. J., and Fairall, C. W.: On the exchange of momentum over the open ocean, J Phys Oceanogr, 43, 1589 - 1610, 2013.

Espy, J. P.: Essays on Meteorology, No. IV: North East Storms, Volcanoes, and Columnar Clouds, Journal of the Franklin Institute, 22, 239 - 246, 1836.

Fairall, C. W., Bradley, E. F., Rogers, D. P., Edson, J. B., and Young, G. S.: Bulk parameterization of air–sea fluxes in TOGA COARE, J. Geophys. Res. Atmos., 101, 3747 - 3767, 1996.

Fairall, C. W., White, A. B., Edson, J. B., and Hare, J. E.: Integrated Shipboard Measurements of the Marine Boundary Layer, J Atmos Ocean Tech, 14, 338 - 359, 1997.

Fairall, C. W., Bradley, E. F., Hare, J. E., Grachev, A. A., and Edson, J. B.: Bulk parameterization of air-sea fluxes: Updates and verification for the COARE algorithm, J Climate, 16, 571 - 591, 2003.

Fratantoni, D. M., and Glickson, D. A.: North Brazil Current Ring Generation and Evolution Observed with SeaWiFS, J Phys Oceanogr, 32, 1058 - 1074, 2002.

Hormann, V., Centurioni, L. R., and Reverdin, G.: Evaluation of drifter salinities in the subtropical North Atlantic, J Atmos Ocean Tech, 32, 185 - 192, 2015.

Liu, D., Wang, Y., Wang, Z., and Zhou, J.: The Three-Dimensional Structure of Transatlantic African Dust Transport: A New Perspective fom CALIPSO LIDAR Measurements, Adv Meteorol, 2012, 10.1155/2012/850704, 2012.

Löffler-Mang, M., and Joss, J.: An optical disdrometer for measuring size and velocity of hydrometeors, J Atmos Ocean Tech, 17, 130 - 139, 2000.

Malm, W. C., Sisler, J. F., Huffman, D., Eldred, R. A., and Cahill, T. A.: Spatial and seasonal trends in particle concentration and optical extinction in the United States, J. Geophys. Res. Atmos., 99, 1347 - 1370, 1994.

Minnett, P., Knuteson, R. O., Best, F., and Osborne, B. J.: The Marine-Atmospheric Emitted Radiance Interferometer (M-AERI), a high-accuracy, sea-going infrared spectroradiometer, J Atmos Ocean Tech, 18, 94 - 1013, 2001.

Mojica, K., and Gaube, P.: Estimates of mixing and mixed layer depth in the Western North Atlantic, Frontiers, submitted, 2020.

Moran, K., Pezoa, S., Fairall, C. W., Williams, C., Ayers, T., Brewer, A., Szoeke, S. P. d., and Ghate, V.: A Motion-Stabilized W-Band Radar for Shipboard Observations of Marine Boundary-Layer Clouds. , Boundary Layer Meteorology, 143, 3 - 24, 2012.

Petit, R. H., Legrand, M., Jankowiak, I., Molimie, J., Asselin de Beauville, C., Marion, G., and Mansot, J. L.: Transport of Saharan dust over the Caribbean islands: Study on an event, J. Geophys. Res. Atmos., 110, 10.1029/2004JD004748, 2005.

Pincus, R., Fairall, C. W., Bailey, A., Chen, H., Chuang, P. Y., Boer, G. d., Feingold, G., Henze, D., Kazil, J., Kalen, Q. T., Leandcro, M., Lundry, A., Moran, K., Naeher, D. A., Patel, A. J., Pezoa, S., Popstefanija, I., Warnecke, J., and Zuidema, P.: Observations from the NOAA research aircraft during the ATOMIC Earth System Science Data Discussion, https://doi.org/10.5194/essd-2021-11, 2021.

Pöhlker, M. L., Ditas, F., Saturno, J., Klimach, T., de Angelis, I. H., Araujo, A. C., Brito, J., Carbone, S., Cheng, Y., Chi, X., Ditz, R., Gunthe., S. S., Holanda, B. A., Kandler, K., Kesselmeier, J., Konemann, T., Kruger, O. O., Lavric, J. V., Martin, S. T., Mikhailov, E., Moran-Zuloaga, D., Rizzo, L. V., Rose, D., Su, H., Thalman, R., Walter, D., Wang, J., Wolff, S., Barbosa, H. M. J., Artaxo, P., Andreae, M. O., Poschl, U., and Pohlker, C.: Long-term observations of cloud condensation nuclei over the Amazon rain forest – Part 2: Variability and characteristics of biomass burning, long-range transport, and pristine rain forest aerosols, Atmos Chem Phys, 18, 10289 - 10331, 2018.

Prospero, J. M., and Mayol-Bracero, O. L.: Understanding the transport and impact of African dust on the Caribbean Basin, Bulletin of the American Meteological Society, 94, 1329 - 1337, 2013.

Quinn, P. K., Bates, T. S., Coffman, D. J., Upchurch, L., Moore, R., Ziemba, L. D., Bell, T. G., Saltzman, E. S., Graff, J., and Behrenfeld, M. J.: Seasonal variations in western North Atlantic remote marine aerosol properties, J. Geophys. Res. Atmos., 124, 14240 - 14261, 2019.

1087   Rose, D., Gunthe, S. S., Mikhailov, E., Frank, G. P., Dusek, U., Andreae, M. O., and Poschl, U.:
1088   Calibration and measurement uncertainties of a continuous-flow cloud condensation nuclei
1089   ounter (DMT-CCNC): CCN activation of ammonium sulfate and sodium chloride aerosol
1090   particles in theory and experiment, Atmos Chem Phys, 8, 1153 - 1179, 2008.
1091   Schroeder, P., Brewer, W. A., Choukulkar, A., Weickmann, A., Zucker, M., Holloway, M. W.,
1092   and Sandberg, S.: A Compact, Flexible, and Robust Micropulsed Doppler Lidar, J Atmos Ocean
1093   Tech, 37, 1387 - 1402, 2020.
1094   Smirnov, A., Holben, B. N., Slutsker, I., D.M.Giles, McClain, C. R., Eck, T. F., Sakerin, S. M.,
1095   Macke, A., P.Croot, Zibordi, G., Quinn, P. K., Sciare, J., Kinne, S., Harvey, M., Smyth, T. J.,
1096   Piketh, S., Zielinski, T., Proshutinsky, A., Goes, J. I., Nelson, N. B., Larouche, P., Radionov, V.
1097   F., Goloub, P., Moorthy, K. K., Matarrese, R., Robertson, E. J., and Jourdin, F.: Maritime
1098   Aerosol Network as a component of Aerosol Robotic Network, J. Geophys. Res. Atmos., 114,
1099   D06204, doi:10.1029/2008JD011257, 2009.
1100   Stephan, C., Schnitt, S., Schulz, H., Bellenger, H., Szoeke, S. P. d., Acquistapace, C., Baier, K.,
1101   Dauhut, T., Laxenaire, R., Morfa-Avalos, Y., Person, R., Quinones-Melendez, E., Bagheri, G.,
1102   Bock, T., Daley, A., Guttler, J., Helfer, K. C., Los, S. A., Neuberger, A., Rottenbacher, J., Raeke,
1103   A., Ringel, M., Ritchel, M., Sadoulet, P., Schirmacher, I., Stolla, M. K., Wright, E., Charpentier,
1104   B., Doerenbecher, A., Wilson, R., Jansen, F., Kinne, S., Reverdin, G., Speich, S., Bony, S., and
1105   Stevens, B.: Ship- and island-based atmospheric soundings from the 2020 EUREC4A field
1106   campaign, Earth System Science Data, under review, 2020.
1107   Stevens, B., Farrell, D., Hirsch, L., Jansen, F., Nuijens, L., Serikov, I., Brugmann, B., Forde, M.,
1108   Linne, H., Lonitz, K., and Prospero, J. M.: The Barbados Cloud Observatory: Anchoring
1109   Investigations of Clouds and Circulation on the Edge of the ITCZ, Bulletin of the American
1110   Meteological Society, 97, 787 - 801, 2016.
1111   Stevens, B., Bony, S., Farrell, D., Ament, F., Blyth, A., Fairall, C. W., Karstensen, J., Quinn, P.
1112   K., Speich, S., and e.t., a.: European project ElUcidating the RolE of Cloud-Circulation Coupling
1113   in ClimAte (EUREC4A), Earth System Science Data, submitted, 2020.
1114   Szczodrak, M., Minnett, P. J., Nalli, N. R., and Feltz, W. F.: Profiling the Lower Troposphere
1115   over the Ocean with Infrared Hyperspectral Measurements of the Marine-Atmosphere Emitted
1116   Radiance Interferometer, J Atmos Ocean Tech, 24, 390 - 402,
1117   https://doi.org/10.1175/JTECH1961.1., 2007.
1118   Thomson, J.: Wave Breaking Dissipation Observed with SWIFT Drifters, J Atmos Ocean Tech,
1119   29, 1866--1882, 10.1175/JTECH-D-12-00018.1, 2012.
1120   Thomson, J., and Girton, J.: Sustained Measurements of Southern Ocean Air-Sea Coupling from
1121   a Wave Glider Autonomous Surface Vehicle, Oceanography Magazine, 30, 104-109, 2017.
1122   Thomson, J., Girton, J. B., Jha, R., and Trapani, A.: Measurements of Directional Wave Spectra
1123   and Wind Stress from a Wave Glider Autonomous Surface Vehicle, J Atmos Ocean Tech, 35,
1124   347-363, 2018.
1125   Thomson, J., Moulton, M., de Klerk, A., Talbert, J., Guerra, M., Kastner, S., Smith, M.,
1126   Schwendeman, M., Zippel, S., and Nylund, S.: A new version of the SWIFT platform for waves,
1127   currents, and turbulence in the ocean surface layer, IEEE/OES Workshop on Currents, Waves,
1128   and Turbulence Measurements, 2019,
1129   Tsamalis, C., Chedin, A., Pelon, J., and Capelle, V.: The seasonal vertical distribution of the
1130   Saharan Air Layer and its modulation by the wind, Atmos Chem Phys, 13, 11235 - 11257, 2013.
1131   Vial, J., Bony, S., Dufresne, J. L., and Roehrig, R.: Coupling between lower-tropospheric
1132   convective mixing and low-level clouds: Physical mechanisms and dependence on convection

scheme, Journal of Advances in Modeling Earth Systems, 8, https://doi.org/10.1002/2016MS000740, 2016.

Weller, R. A.: Observing surface meteorology and air sea fluxes, in: Observing the Oceans in Real Time, edited by: Venkatesan, R., Tandon, A., D'Asaro, E., and Atmanand, M. A., Springer International, 17 - 35, 2018.

Wex, H., Dieckmann, K., Roberts, G., Conrath, T., Izaguirre, M. A., Hartmann, S., Herenz, P., Schafer, M., Ditas, F., Schmeissner, T., Henning, S., Wehner, B., Holger-Siebert, H., and Stratmann, F.: Aerosol arriving on the Caribbean island of Barbados: physical properties and origin, Atmos Chem Phys, 16, 14107 - 14130, 2016.

Whittlestone, S., and Zahorowski, W.: Baseline radon detectors for shipborad use: Development and deployment in the First Aerosol Characterization Experiment (ACE-1), J. Geophys. Res. Atmos., 103, 16743-16751, 1998.

Zhang, D., Cronin, M. F., Meinig, C., Farrar, J. T., Jenkins, R., Peacock, D., Keene, J., Sutton, A., and Yang, Q.: Comparing Air-sea flux measurements from a new unmanned surface vehicle and proven platforms during the SPURS-2 Field Campaign, Oceanography, 32, 122 - 133, 2019.

Zuidema, P.: Overview of ATOMIC, in preparation, 2021.